Revised and Resubmitted to Journal of Computational Physics

Towards shock-stable and accurate hypersonic heating computations: A new pressure flux for AUSM-family schemes

Keiichi Kitamura[1] and Eiji Shima

JAXA's Engineering Digital Innovation (JEDI) Center, Japan Aerospace Exploration Agency, 3-1-1 Yoshinodai, Sagamihara, Kanagawa, 252-5210, Japan

Abstract

Hypersonic heating computations are still challenging due to difficulties in "A) robust capturing of shockwaves" and "B) accurate prediction of heating." Based on our numerical survey for A), we found that the dissipation inside the numerical shock wave structure (where no physical or mathematical explanation is valid) must be proportional to Mach number, in contrast to Mach independent dissipation provided by conventional AUSM fluxes. Then, we developed schemes that have those two properties above by combining a) a proposed pressure flux (having Mach-proportional dissipation within numerical shock), and b) a mass flux of an all-speed AUSM-family scheme (SLAU, AUSM$^+$-up or LDFSS2001). The new schemes, called "SLAU2," "AUSM$^+$-up2," and "LDFSS2001-2," are applied to numerical tests, and their desired performances are demonstrated for a wide spectrum of Mach numbers, including hypersonic heating (for the latter two schemes), a low speed flow, and 3D aerodynamic applications.

Keywords: Hypersonic Heating; All-speed scheme; Low-dissipation; Preconditioning; Carbuncle; AUSM-family

1. Introduction

Hypersonic heating computations are still challenging due to difficulties in "A) robust capturing of shockwaves" and "B) accurate prediction of heating," in spite of great progresses of both CFD (Computational Fluid Dynamics) methods and computer technologies. The issue A) is represented by "carbuncle phenomenon (Fig. 1) [1-4]." It is very easy from simple examples such as in Fig.1 to find a "correct" solution; however, in practical simulations involving complex geometries with complex flow phenomena (Ref. [5], for instance), it is almost impossible to identify such anomalies, if any. This difficulty degrades the reliability of currently available CFD methods and afflicts the use of them in hypersonic flows.

Those anomalies are sometimes called "shock instabilities [6,7]," because they occur at numerically resolved shock waves by finite-volume, shock-capturing methods [2]. Usage of those terminologies are scattered even among the related-researchers, and a part of the reasons lies in the fact that it is still an open question whether the carbuncle phenomenon is a numerical artifact or not. Until almost a decade ago, the carbuncle had been believed as a

[1] corresponding author; tel: +81-52-789-3394, e-mail address: kitamura@fluid.nuae.nagoya-u.ac.jp; Research Fellow of the Japan Society for the Promotion of Science (JSPS), and Visiting Researcher at NASA Glenn Research Center, Cleveland, OH 44135, USA, and currently Assistant Professor at Nagoya University, Furo-cho, Chikusa-ku, Nagoya, Japan.

numerical anomalous solution [2]; however, more recent studies [8-11] argued that the carbuncle was a rather mathematical or physical one.

Recently, in an attempt to resolve this argument, Liou [12] tried to categorize carbuncle as a purely numerical artifact which appeared only for certain flux functions, and therefore, claimed that it was 'operationally' avoidable by, for instance, AUSM$^+$-up flux [13]. This holds for most cases, but there are a few exceptions: When a large number of cells are piled up in a shock-parallel direction [14], carbuncle phenomenon does appear even when AUSM$^+$-up [13] or Van Leer's flux-vector-splitting (FVS) [15] is used, as shown in Fig. 2. Thus, we believe this dispute has not been settled yet.

In the present study, we take the viewpoint that the shock anomalies are at least partly caused by the lack of mathematical expression for internal shock structure by the governing equations [14] on the grounds that

- The carbuncle appears as one of the physical solutions, as if a spike is mounted ahead of a blunt-body in a hypersonic flow [16]. This fact excludes the following simple classification: A physical solution is "correct," and a carbuncle solution is unphysical.
- In the real physics, a shock wave has finite thickness and inside structure. From the viewpoint of continuum mechanics, on the other hand, a shock wave is regarded as a zero-thickness discontinuity. Euler equations to be solved are based on the latter, but a numerically captured shock (by shock-capturing methods) usually contains a few (at least one) computational cells forming numerical internal shock structure [17-19].
- The numerical shock structure violates Euler equations and/or the Rankine-Hugoniot relation [18, 19]. Both equations are valid only "across" the shock, not "inside" it. Further discussions are found in Refs. [4, 6, 17, 20].
- There is no reported anomalous solution by a shock-fitting method which produces no shock width [2, 21, 22].

Then, among the scattered terminologies, we had redefined in [23] the shock related anomalous solutions[3] as in Table1, that is, "shock anomalies" are categorized into two phenomena of "shock oscillations" and "shock instabilities." The carbuncle belongs to the latter family and appears only in multi-dimensions. "Oscillations" stand for the oscillatory behaviors of the captured shock, whether in time or space, usually confined within only two cells. Such situations often arise when, in a non-shock-aligned grid, the shock jumps from one set of mesh line to another [14, 24]. The spatially multi-dimensional oscillation is also referred to as "asymmetry."

Anomalies	Oscillations	Instabilities
1D	Y (in time)[2]	N (Not observed yet)
Multi-D	Y (both in time and space)	Y (Carbuncle)

Table 1 Shock anomalies [23]

It is known that 'the shock anomalies should not have any single cause, nor is there any single cure [4].' It is difficult to establish such cures theoretically, because we still have not reached an accepted conclusions for how numerical internal shock structure should be expressed, as stated above. It is also difficult to establish them experimentally, because the anomalies depend on mesh geometry, mesh size, flow Mach number, and specific heat ratio [2, 4, 14]. Kitamura et al. [4, 14] conducted systematic experimental investigations by paying particular attention to flux functions and mesh. They concluded that one dimensional (1D) and multi-dimensional (Multi-D) shock anomalies appeared independently, and any existing flux functions suffered from either of them.

As a starting point of this work, SLAU [Simple Low-dissipation AUSM (Advection Upstream Splitting Method)] flux, recently developed by the authors [25], will be tested first as in Refs. [4, 14]. The SLAU is one of low-dissipation schemes of AUSM-family, and free from any tunable parameters. SLAU showed an excellent performance at low speeds [25, 26], not to mention in moderate speed regimes; but as in other flux functions, anomalous behaviors were observed at shocks under some circumstances in hypersonic flows. Specifically, it was left ambiguous how to deal with shock internal structure, e.g., speed of sound inside the shock.

In the first half of the present paper, after brief explanations for the computational methods, fundamental discriptions for "cell-interfacial speed of sound," denoted as $c_{1/2}$, will be given. The $c_{1/2}$ is the speed of sound numerically defined at a cell-interface, and usually used to calculate an AUSM-family numerical flux [13, 24, 25] (see Figure 3). We will focus on the role of $c_{1/2}$, and the numerical tests in Refs. [4, 14] will be conducted for SLAU and other fluxes.

[2] The authors used the term "1D carbuncle" in the earlier work [4], but here we abandoned this expression to avoid confusions.

[3] Although the conventional term "shock instabilities" is used in our earlier publications, we will use the new, recently updated definitions of "shock anomalies (Table 1)" in the rest of the paper.

The definition of $c_{1/2}$ is, as mentioned above, one of critical questions of what the numerical shock structure should be, since $c_{1/2}$ is usually left as a scheme's parameter while the other physical quantities at the cell-interfaces such as primitive variables can be somehow interpolated from cell-center values. Naturally, the $c_{1/2}$ has many options, e.g., arithmetic or geometric average, and it will be explored in the present work which expression would be suitable for SLAU or other AUSM-family fluxes for improvements in their robustness/stability against the captured shocks. Since $c_{1/2}$ inside the shock is purely a numerical quantity (where no physical or mathematical explanation is justifiable), numerical experiments are considered to be the only way to find its proper value.

Ref. [27] is, to the best of the authors' knowledge, the only one in which the effects of $c_{1/2}$ was studied for high Mach numbers. Liou and Edwards [27] revealed that slight modifications of $c_{1/2}$ could influence stability of the shock for AUSM$^+$ [24] and even Roe flux [28] or Van Leer's FVS [15]. However, their discussions were limited to one dimension and the most of their work was dedicated to low speed flow extensions. As demonstrated in Ref. [4], however, 1D and multi-dimensional shock anomalies should be considered differently, and that will be done in the present work.

Then, based on the findings, the pressure flux of SLAU will be modified to have more proper amount of dissipation inside the shock: Modification of dissipation term containing $c_{1/2}$ turns out to be good enough. As will be demonstrated from numerical examples, the improved scheme, named SLAU2, is promising for a broad spectrum of flow speed regimes.

For hypersonic heating computations, however, even this scheme needs further improvement, as will be demonstrated later (and also reported by Hiroaki Nishikawa, National Institute of Aerospace, and Jeffery White, NASA Langley, in private communication).

The heating issue "B) accurate prediction of heating" has usually been discussed together with "A) robust capturing of shockwaves" [14,29,30], since B) is considered to be strongly related to A) and shock anomalies actually contaminate the post-shock solutions including wall heating significantly. The authors previously proposed the following three properties for accurate heating computations and investigated various numerical flux functions in Ref. [14]:

A) Robustness against shock anomalies

B-1) Total enthalpy preserving

B-2) Boundary-layer resolving (An ability of the Euler solver to sharply resolve contact discontinuities)

In actuality, and unfortunately, there found no method which satisfied all the three properties in a strong sense; specifically, A) is not perfectly guaranteed even by AUSM$^+$-up [13] or Van Leer's FVS [15], as seen in Fig. 2 [14]. Nevertheless, at least under certain conditions, AUSM-family schemes such as AUSM$^+$[24] achieved A) and such schemes are designed to satisfy B-1) and B-2), and thus, produced good heating profiles over the wall. Therefore, if one is interested in not only the stagnation point heating, but also in its distributions, the following condition should be added to A), B-1), and B-2):

B-3) Smooth representation of heating profiles (if the other conditions are guaranteed)

AUSM-family schemes are often used for hypersonic flows, primarily due to their robustness and simplicity. Generally, an AUSM-family flux is formulated to be composed of a) pressure flux and b) mass flux. Each component has its own contribution to the solution calculated from cell-interfacial differences of pressure and mass, respectively. Across the shock, the mass flux is constant according to the mass conservation law, but pressure has discontinuous jump, thus, a) pressure flux must have a greater contribution. On the other hand, as for the wall heating in the (attached) boundary-layer, pressure is usually constant normal to the wall, and hence, b) mass flux should have a larger impact.

Therefore, in the second half of this article, we will consider to design numerical flux functions which satisfy both A) and B) by simply combining a) pressure flux of SLAU2 having excellent performance in A), and b) mass flux of another AUSM-family scheme such as AUSM$^+$-up [13] or LDFSS (Low Diffusion Flux Splitting Scheme) 2001 [31] having properties B1), B2), and B3).

In addition, we remind that SLAU [25], SLAU2, AUSM$^+$-up and LDFSS2001 are all-speed schemes that satisfy

C) Low dissipation at low speeds

Thus, the new schemes are also supposed to have C). This will also be demonstrated in numerical examples.

We are aware of recent progresses in the related area: BGK (Bhatnagar-Gross-Krook)-equation-based finite-volume method (FVM) [32] by Xu et al. and shock-fitting approach by Paciorri and Bonfiglioli in [22]. With the help of other strategies than a conventional shock-capturing scheme, they achieved some success in suppression of shock anomalous solutions. These approaches are interesting, however, it is still unclear whether they will provide accurate heating prediction and will be free from the two heating issues stated above on any conditions. Furthermore, many CFD practitioners are still using and heavily relying upon shock-capturing FVM codes because of their simplicity in algorithm and coding both. Our present methods are the ones that fulfill their desire.

The paper is organized as follows: Section 2 gives brief explanations for the computational methods; "cell-interfacial speed of sound," $c_{1/2}$, will be introduced and studied in Section 3, with development of SLAU2 scheme along with a new pressssure flux having a proper ammount of dissipation at hypersonic speed. Then, its performance against shock anomalies will be also demonstrated. Note that in surveying $c_{1/2}$ inside the shock, we will take numerical approach rather than (impossible) mathematical or physical explanations. In Section 4, the same pressure flux will be applied to other well-known AUSM-family shemes, i.e., AUSM$^+$-up and LDFSS2001, leading to further developments: "AUSM$^+$-up2" and "LDFSS2001-2." Section 5 deals with the two heating issues A) and B) in which the new flux functions are tested, and Section 6 presents other numerical tests, including a low speed flow, a 3D heating test, and a practical application to a rocket configuration. Section 7 will conclude the present work.

2. Numerical Method

2.1 Governing equations

The governing equations are the compressible Navier-Stokes equations as follows, including the preconditioning matrix $\mathbf{\Gamma}$ of Weiss and Smith [33], which is simply eliminated in the non-preconditioned form:

$$\mathbf{\Gamma}\frac{\partial \mathbf{Q}}{\partial t}+\frac{\partial \mathbf{F}_k}{\partial x_k}=0 \qquad \text{: Euler} \tag{2.1a}$$

$$\mathbf{\Gamma}\frac{\partial \mathbf{Q}}{\partial t}+\frac{\partial \mathbf{F}_k}{\partial x_k}=\frac{\partial \mathbf{F}_{vk}}{\partial x_k} \qquad \text{: Navier-Stokes} \tag{2.1b}$$

$$\mathbf{Q}=\begin{bmatrix}\rho\\ \rho u_l\\ \rho E\end{bmatrix},\quad \mathbf{F}_k=\begin{bmatrix}\rho u_k\\ \rho u_l u_k+p\delta_{lk}\\ \rho u_k H\end{bmatrix},\quad \mathbf{F}_{vk}=\begin{bmatrix}0\\ \tau_{lk}\\ u_m\tau_{mk}+\kappa\dfrac{\partial T}{\partial x_k}\end{bmatrix} \tag{2.1c}$$

$$\tau_{lk}=\mu\left(\frac{\partial u_l}{\partial x_k}+\frac{\partial u_k}{\partial x_l}\right)-\frac{2}{3}\mu\frac{\partial u_n}{\partial x_n}\delta_{lk} \tag{2.1d}$$

where ρ is the density, u_l velocity components in Cartesian coordinates, E total energy, p pressure, H total enthalpy ($H = E + (p/\rho)$), and T temperature. The working gas is air approximated by the calorically perfect gas model with the specific heat ratio γ=1.4. The Prandtl number is Pr=0.72. The molecular viscosity μ and thermal conductivity κ are related as κ=$c_p\mu$/Pr where c_p is specific heat at constant pressure. The viscosity μ is calculated by the Sutherland's formula for hypersonic heating problems, whereas it is kept constant for others. In the turbulence calculations, molecular viscosity μ is replaced by (μ+μ_t), where μ_t is turbulence viscosity. Likewise, κ is replaced by (κ+$c_p\mu_t$/Pr_t), where Pr_t is the turbulent Prandtl number, 0.89.

These equations are solved with a finite-volume code, and can be written in the delta form as:

$$\frac{V_i}{\Delta t_i}\Delta\mathbf{Q}_i+\mathbf{\Gamma}_i^{-1}\sum_j(\mathbf{F}_{i,j}-\mathbf{Fv}_{i,j})S_{i,j}=0 \tag{2.2}$$

where V_i stands for the volume of the cell i, Δt_i the (local) time step, $\Delta\mathbf{Q}_i$ change of conservative variables in time, $\mathbf{F}_{i,j}$ and $\mathbf{F}_{vi,j}$ the inviscid (Euler) and viscous fluxes through the cell-interface $S_{i,j}$ (which separates the cell i and its neighbor cell j), respectively (see Fig. 4).

2.2 Numerical method

The following methods are used for computations herein, if not mentioned otherwise.

As for spatial discretization, the primitive variables at cell centers are used also as cell-interfacial values for spatially first order cases; In second order simulations, the primitive variables at each cell-interface are interpolated

by using MUSCL (Monotone Upstream-centered Schemes for Conservation Laws) reconstruction [34] with Van Albada's limiter [35]. Then, inviscid fluxes at the cell-interface are calculated from the AUSM-family flux functions introduced in the next subsection.

2.3 AUSM-family numerical flux functions

The following methods are used for computations herein, if not mentioned otherwise.

Inviscid numerical fluxes at cell-interfaces $\mathbf{F}_{i,j}$ (denoted also as $\mathbf{F}_{1/2}$ hereafter) are calculated by one of the following AUSM-family fluxes [13, 25, 31]. AUSM-family schemes originate from Van Leer's FVS [15] and there have been many variants published so far (Fig. 3).

2.3.1 SLAU

SLAU scheme developed by Shima and Kitamura [25], one of AUSM-family schemes, is briefly explained first. The cell-interface flux $\mathbf{F}_{1/2}$ is calculated as:

$$\mathbf{F}_{1/2} = \frac{\dot{m} + |\dot{m}|}{2}\boldsymbol{\Psi}^{+} + \frac{\dot{m} - |\dot{m}|}{2}\boldsymbol{\Psi}^{-} + \tilde{p}\mathbf{N} \tag{2.3a}$$

$$\boldsymbol{\Psi} = (1,\, u,\, v,\, w,\, H)^T, \quad \mathbf{N} = (0,\, n_x,\, n_y,\, n_z,\, 0)^T \tag{2.3b}$$

where "+" and "-" denote the left (L) and right (R) states at the cell-interface, respectively (Fig. 2). Then, a) pressure flux is

$$\tilde{p} = \frac{p_L + p_R}{2} + \frac{f_p^{+}\big|_{\alpha=0} - f_p^{-}\big|_{\alpha=0}}{2}(p_L - p_R) + (1-\chi)\left(f_p^{+}\big|_{\alpha=0} + f_p^{-}\big|_{\alpha=0} - 1\right)\frac{p_L + p_R}{2} \tag{2.3c}$$

$$\chi = (1-\hat{M})^2 \tag{2.3d}$$

$$\hat{M} = \min\left(1.0, \frac{1}{c_{1/2}}\sqrt{\frac{u_L^{\,2} + v_L^{\,2} + w_L^{\,2} + u_R^{\,2} + v_R^{\,2} + w_R^{\,2}}{2}}\right) \tag{2.3e}$$

$$f_p^{\pm}\big|_{\alpha=0} = \begin{cases} \dfrac{1}{2}\left(1 \pm sign(M)\right), & if\ |M| \ge 1 \\ \dfrac{1}{4}(M \pm 1)^2(2 \mp M), & otherwise \end{cases} \tag{2.3f}$$

$$M = \frac{V_n}{c_{1/2}} = \frac{un_x + vn_y + wn_z}{c_{1/2}} \tag{2.3g}$$

$$c_{1/2} = \bar{c} = \frac{c_L + c_R}{2} \tag{2.3h}$$

and b) mass flux is

$$\dot{m} = \frac{1}{2}\left\{\rho_L\left(V_{nL} + |\bar{V}_n|^{+}\right) + \rho_R\left(V_{nR} - |\bar{V}_n|^{-}\right) - \frac{\chi}{c_{1/2}}\Delta p\right\} \tag{2.3i}$$

$$|\bar{V}_n|^{+} = (1-g)\,|\bar{V}_n| + g\,|V_{nL}|, \quad |\bar{V}_n|^{-} = (1-g)\,|\bar{V}_n| + g\,|V_{nR}| \tag{2.3j}$$

$$|\bar{V}_n| = \frac{\rho_L|V_{nL}| + \rho_R|V_{nR}|}{\rho_L + \rho_R} \tag{2.3k}$$

$$g = -\max\left[\min\left(M_L, 0\right), -1\right] \cdot \min\left[\max\left(M_R, 0\right), 1\right] \quad \in [0, 1] \tag{2.3l}$$

Note in Eq. (2.3h) that the interface speed of sound $c_{1/2}$ is defined as arithmetic average of c_L and c_R. This scheme relies upon no prescribed parameters, such as cutoff Mach number. This feature differentiates the scheme from other well-known all-speed schemes, and is desirable for flows having no uniform Mach numbers, e.g, internal flows.

2.3.2 AUSM$^+$-up

AUSM$^+$-up, the latest version of AUSM by Liou [13], is briefly described. As in SLAU, the numerical flux is expressed as in Eq. (2.3a) and (2.3b), but a) pressure flux is given by

$$\tilde{p} = f_p^+\big|_\alpha \, p_L + f_p^-\big|_\alpha \, p_R + p_u \tag{2.4a}$$

$$f_p^\pm\big|_\alpha = \begin{cases} \frac{1}{2}\left(1 \pm sign(M)\right), & if\ |M| \ge 1 \\ \frac{1}{4}(M \pm 1)^2 (2 \mp M) \pm \alpha M \left(M^2 - 1\right)^2, & otherwise \end{cases} \tag{2.4b}$$

$$p_u = -K_u \beta_+ \beta_- (\rho_L + \rho_R)(f_a c_{1/2})(V_n^- - V_n^+) \tag{2.4c}$$

where $c_{1/2}$ is calculated as

$$c_{1/2} = \min(\tilde{c}_L, \tilde{c}_R), \quad \tilde{c}_L = c^{*2} / \max(c^*, V_n^+), \quad \tilde{c}_R = c^{*2} / \max(c^*, -V_n^-) \tag{2.4d}$$

$$c^{*2} = \frac{2(\gamma - 1)}{(\gamma + 1)} H \tag{2.4e}$$

The full description of b) mass flux and tunable parameters such as K_u are provided in Appendix. Furthermore, AUSM$^+$-up requires another user-specified value, that is, uniform Mach number M_∞.

2.3.3 LDFSS2001

The key elements of LDFSS2001 scheme [31] proposed by Edwards are explained here. This scheme is written as

$$\tilde{\mathbf{F}} = \dot{m}^+ \boldsymbol{\Psi}^+ + \dot{m}^- \boldsymbol{\Psi}^- + \tilde{p}\mathbf{N} \tag{2.5a}$$

$$\boldsymbol{\Psi} = (1, u, v, w, H)^T, \quad \mathbf{N} = (0, n_x, n_y, n_z, 0)^T \tag{2.5b}$$

and a) pressure flux is

$$\tilde{p} = \frac{p^+ + p^-}{2} + \frac{f_p^+\big|_{\alpha=0} - f_p^-\big|_{\alpha=0}}{2}\left(p^+ - p^-\right) + \bar{\rho} V_{ref,1/2}^2 \left(f_p^+\big|_{\alpha=0} + f_p^-\big|_{\alpha=0} - 1\right) \tag{2.5c}$$

$$f_p^\pm\big|_{\alpha=0} = \begin{cases} \frac{1}{2}\left(1 \pm sign(M)\right), & if\ |M| \ge 1 \\ \frac{1}{4}(M \pm 1)^2 (2 \mp M), & otherwise \end{cases} \tag{2.5d}$$

where the cell-interfacial speed of sound, reference velocity, and other quantities are given as follows:

$$M_{L/R} = V_n^\pm / \tilde{c}_{1/2}, \quad \tilde{c}_{1/2} = \sqrt{\tilde{c}_L \cdot \tilde{c}_R}, \quad \tilde{c}_{L/R} = \frac{\sqrt{V_n^{\pm 2}\left(1 - M_{ref}^2\right)^2 + 4V_{ref}^2}}{1 + M_{ref}^2} \tag{2.5e}$$

$$M_{ref}^2 = V_{ref}^2 / {c_{1/2}}^2, \quad V_{ref}^2 = \min\left({c_{1/2}}^2, \max\left(|\vec{V}|^2, V_\infty^2\right)\right), \quad |\vec{V}|^2 = u^2 + v^2 + w^2 \tag{2.5f}$$

$$c_{1/2} = \min(c_L, c_R), \quad c_{L/R} = c^{*2} / \max\left(c^*, |V_n^\pm|\right), \quad c^{*2} = \frac{2(\gamma - 1)}{(\gamma + 1)} H \tag{2.5g}$$

where the uniform velocity V_∞ should be specified by a user. The mass flux is fully described also in Appendix.

2.3.4 AUSM$^+$

For reference, AUSM$^+$ [24], a predecessor of AUSM$^+$-up, is also reviewed. With Eqs. (2.3a) and (2.3b),

$$\tilde{p} = f_p^+\big|_\alpha\, p_L + f_p^-\big|_\alpha\, p_R \tag{2.6a}$$

$$f_p^\pm\big|_\alpha = \begin{cases} \dfrac{1}{2}\left(1 \pm sign(M)\right), & if\ |M| \ge 1 \\ \dfrac{1}{4}(M \pm 1)^2(2 \mp M) \pm \alpha M\left(M^2-1\right)^2, & otherwise \end{cases} \tag{2.6b}$$

where α = 3/16, and $c_{1/2}$ is given by Eq. (2.5g) as in LDFSS2001. Thus, differences from AUSM$^+$-up lie in the definition of speed of sound, Eq. (2.5g), and elimination of some parameters such as p_u. Note that this scheme is not an all-speed scheme, so exhibits severe numerical errors at low speeds [13, 26].

3. SLAU2: Its development based on role of interfacial speed of sound

3.1 Interfacial speed of sound

As seen in the last section, most of AUSM-family schemes such as AUSM$^+$-up [13], LDFSS2001 [31], and SLAU [25] need speed of sound at the cell interface, $c_{1/2}$, and there is some degree of freedom for choosing it [24].

A simple arithmetic averaging in Eq. (2.3h), for example, works well for SLAU for general cases. On the other hand, another definition in Eq. (2.5g) was used for AUSM$^+$ (and also for LDFSS2001) to capture normal shock properly. Other choices were also possible for AUSM$^+$ [24], such as

$$c_{1/2} = \max\left(\tilde{c}_L, \tilde{c}_R\right), \quad \tilde{c} = c^{*2}/\max\left(c^*, |V_n|\right) \tag{3.1a}$$

or geometric average,

$$c_{1/2} = \sqrt{c_L c_R} \tag{3.1b}$$

or even Roe-average,

$$c_{1/2} = \hat{c} = \sqrt{(\gamma-1)\left(\hat{H} - 0.5\hat{q}^2\right)}, \quad \hat{q}^2 = \hat{u}^2 + \hat{v}^2 + \hat{w}^2 \tag{3.1c}$$

The choice of the interface sound of speed $c_{1/2}$ has little effect on low or moderate Mach number flows (M<1), obviously because c_L and c_R are exactly or almost equal to each other. However, as will be shown later, it has significant influence on numerical stability/robustness of the schemes at a shock at higher Mach numbers. Ref. [27] is, to the best of the authors' knowledge, the only one in which the effects of $c_{1/2}$ was studied for high Mach number flows. Liou and Edwards [27] revealed that slight modifications of $c_{1/2}$ in Eq. (2.5g) to the form of Eq.(3.1a) generally stabilized the shock for AUSM$^+$ and even Roe flux or Van Leer's FVS. However, their discussions were limited to one dimension and the most of their work was dedicated to low speed flows. As demonstrated in Ref. [4], 1D and multi-dimensional shock anomalies should be considered separately, and this is done in the present work.

Figure 5 shows an example of how $c_{1/2}$ differs depending on its definitions for a Mach 6 normal shock. The abscissa stands for index of the cell-interface [Note: i-th cell-interface is located between i-th and (i+1)-th cells], and the ordinate the cell-interfacial speed of sound, $c_{1/2}$, standardized by the freestream (= preshock) speed of sound, c_∞. The normal shock is placed exactly at the cell-interface between i=12 and 13 cells (= 12th interface) in the 50 cells of a one-dimensional computational grid (shown later in Fig. 6). Then, the $c_{1/2}$ is extracted at the very beginning of the computation (before the temporal evolution in the first timestep)[4] for each definition.

It is seen from the graph that the interfacial speed of sound, $c_{1/2}$, can take various values between c_L and c_R "inside" the shock (i.e., at 12th interface), while it is uniform elsewhere. The arithmetic averaged value from Eq. (2.3h), 1.90895, SLAU default, is in the middle of the five definitions, and the Eq. (2.5g), AUSM$^+$ default, gave 1.13889 which is approximately 60% of the arithmetic averaged value. Since these numbers displayed here are standardized by uniform (left) velocity, this difference in actual numbers will increase with Mach number (e.g, at a stronger shock). Note that the interface speed of sound $c_{1/2}$ controls the amount of numerical diffusion in some of the numerical flux function (the third term of Eq. (2.3c), for instance). Effects of changing these definitions on the shock stability/robustness of the schemes will be examined in the next section.

We remind the readers of that this modification of $c_{1/2}$ is only applicable to shock internal structure; the speed of sound "outside" the shock is not usually affected since c_L and c_R are the same.

3.2 Role of interfacial speed of sound: steady normal shock numerical test

[4] Thus, these calculated values of $c_{1/2}$ are irrelevant to any of numerical methods in the code, such as flux functions. We confirmed hand-calculations yielded the same outputs.

3.2.1 1.5D (one-and-half dimensional) steady normal shock test setup

This problem is called "1.5D (or 1-1/2-D) problem," which was conducted in Ref. [4] to examine how schemes show robustness in capturing a steady normal shock in a two-dimensional rectangular domain (Fig. 6). This setup mimics a close-up view of a hypersonic flow ahead of a stagnation point of a two-dimensional blunt-body, and hence, largely predicts results of such flow computations. In this paper we briefly review the problem and refer to Ref. [4] for details.

As shown in Fig. 6, the computational grid comprises 50×25 cells evenly spaced without perturbations. A steady shock that includes an intermediate state is prescribed with initial conditions for left (L: $i\leq 12$) and right (R: $i\geq 14$) following the Rankine-Hugoniot conditions across the normal shock with the freestream Mach number M_∞=6.0 (V_{ref} = $c_{1/2}$ and M_{ref} = 1 in Eq.(2.5f) of LDFSS2001). The internal shock conditions (M: i=13) are as follows:

1) The density is given as

$$\rho_M = \varepsilon \rho_L + (1-\varepsilon)\rho_R \tag{3.2}$$

where the shock-position parameter ε = 0.0, 0.1, ... , 0.9. The initial shock is imposed exactly on the cell-interface when ε=0.0, for instance, and at the cell-center when ε=0.5.

2) The other variables are calculated based on ρ_M so that all variables lie on the Hugoniot curve. No perturbations are introduced either to the initial condition.

The computations are conducted for 40,000 steps with CFL=0.5. We point out that longer timesteps or a smaller CFL essentially did not affect the solutions. If a scheme is stable for all the shock positions of ε, the scheme are regarded to be as robust as Van Leer's FVS [14]. Typical solutions are shown in Fig. 7:

- '**2**' denotes a stable and symmetric solution with at least three orders of (L2-norm of) density residual reduction.
- '**1**' denotes an asymmetry and/or oscillation of the shock confined within two cells of the shock normal direction.
- '**0**' denotes an unstable solution usually associated with total breakdown of the shock ("carbuncle"). The residual stagnated at a significant value.

3.2.2 Steady normal shock results

Flux functions and $c_{1/2}$ definitions	Test Problem	ε=0.0	0.1	0.2	0.3	0.4	0.5	0.6	0.7	0.8	0.9	Total	
SLAU **(default)**	1D	**2**	**2**	**2**	**2**	**2**	**2**	**2**	**2**	**2**	**2**	**20**	33
$[c_{1/2}= 0.5(c_L+c_R)]$	1.5D	1	**2**	**2**	**2**	1	1	1	1	1	1	13	
SLAU, Eq.(2.5g)	1D	**2**	**2**	**2**	**2**	**2**	**2**	**2**	**2**	**2**	**2**	**20**	35
$[c_{1/2}=\min(c_L^{\sim},c_R^{\sim})]$	1.5D	**2**	**2**	**2**	1	1	1	1	1	**2**	**2**	15	
AUSM$^+$, Eq.(2.3h)	1D	**2**	**2**	**2**	**2**	1	1	**2**	**2**	**2**	**2**	18	32
$[c_{1/2}= 0.5(c_L+c_R)]$	1.5D	**2**	**2**	**2**	**2**	1	1	1	1	1	1	14	
AUSM$^+$ **(default)**	1D	**2**	**2**	**2**	**2**	1	1	1	**2**	**2**	**2**	17	33
$[c_{1/2}=\min(c_L^{\sim},c_R^{\sim})]$	1.5D	**2**	**2**	**2**	**2**	1	1	1	1	**2**	**2**	16	
AUSM$^+$, Eq.(3.1a)	1D	**2**	**2**	**2**	**2**	1	**2**	**2**	**2**	**2**	**2**	19	32
$[c_{1/2}=\max(c_L^{\sim},c_R^{\sim})]$	1.5D	**2**	**2**	1	1	1	1	1	1	1	**2**	13	
AUSM$^+$, Eq.(3.1b)	1D	**2**	**2**	**2**	**2**	1	1	**2**	**2**	**2**	**2**	18	32
$[c_{1/2}=\text{sqrt}(c_L,c_R)]$	1.5D	1	**2**	**2**	**2**	1	1	1	1	1	**2**	14	
AUSM$^+$, Eq.(3.1c)	1D	**2**	**2**	**2**	**2**	1	1	**2**	**2**	**2**	**2**	18	33
$[c_{1/2}=RoeAvg(c_L,c_R)]$	1.5D	**2**	**2**	**2**	**2**	1	1	1	1	1	**2**	15	
Roe, Eq.(3.1c)	1D	1	**2**	**2**	**2**	**2**	**2**	**2**	1	1	1	16	22
$[c_{1/2}= RoeAvg(c_L,c_R)]$	1.5D	0	**2**	**2**	**2**	0	0	0	0	0	0	6	
Roe (E-fix), Eq.(3.1c)	1D	**2**	**2**	**2**	**2**	**2**	**2**	**2**	**2**	**2**	**2**	**20**	20
$[c_{1/2}= RoeAvg(c_L,c_R)]$	1.5D	0	0	0	0	0	0	0	0	0	0	0	

Table 2 1D and 1.5D tests for schemes with various $c_{1/2}$ definitions (ε: shock location parameter [4])

In the present study, SLAU and AUSM$^+$ of AUSM-family fluxes with different $c_{1/2}$ definitions are tested through the 1.5D numerical experiments, as well as its 1D counterparts where only one cell is used for the shock parallel direction [4]. A selection of computations is summarized in Table 2. The results of Roe flux [28] (with and without entropy-fix [36]) are also shown for reference. Total points in terms of shock stability/robustness of each scheme are given in the rightmost column (in 20 points maximum for each test).

The following features are noteworthy from Table 2:

- SLAU and AUSM$^+$ both are more robust against shock anomalies than Roe flux.
- SLAU is always stable (2) for 1D test, but showed some anomalous solutions (1) in 1.5D.
- When $c_{1/2}$ is changed from arithmetic average to that of AUSM$^+$ in which critical speed of sound is used, SLAU shows better performance.
- AUSM$^+$ showed little influence in total points of two tests from change of $c_{1/2}$, by balance of better performance in 1D and degraded stability in 1.5D, or vice versa. For instance, AUSM$^+$ with $c_{1/2}$=max($c_L^{\sim}$,$c_R^{\sim}$) showed more stable 1D results than its default choice as reported in [27], but actually with worse 1.5D results.

In summary, the choice of $c_{1/2}$ influences response of flux functions to the captured shock in either 1D or Multi-D. Particularly, SLAU with $c_{1/2}$ of AUSM$^+$ default, Eq. (2.5g), showed improvement of the shock stability/robustness, whereas for AUSM$^+$ it seems impossible to identify which option is the best. SLAU has numerical dissipation term having $c_{1/2}$ (the third term of Eq. (2.3c)) which is absent in AUSM$^+$. With modification of $c_{1/2}$ of SLAU from arithmetic average to the AUSM$^+$ form, its magnitude is reduced as stated earlier (Fig. 5). From Eqs. (2.3c)-(2.3e) one can easily trace that this reduction of $c_{1/2}$ led to more dissipation in the numerical dissipation term. Thus, it is said that dissipation of original SLAU was insufficient to stabilize Multi-D anomalies, and that more proper amount of dissipation has been fed into the SLAU flux by the current modification. Based on these findings, we will consider further improvement of the SLAU scheme.

3.3 New pressure flux and derivation of SLAU2

For clarity, the pressure flux of SLAU [Eqs. (2.3c)-(2.3e)] are rewritten as follows:

$$\tilde{p} = \frac{p_L + p_R}{2} + \frac{f_p^+ - f_p^-}{2}(p_L - p_R) + \left(1 - \left(1 - \hat{M}\right)^2\right)\left(f_p^+ + f_p^- - 1\right)\frac{p_L + p_R}{2} \tag{3.3a}$$

$$\hat{M} = \min\left(1.0, \frac{1}{c_{1/2}}\sqrt{\frac{u_L^{\,2} + v_L^{\,2} + w_L^{\,2} + u_R^{\,2} + v_R^{\,2} + w_R^{\,2}}{2}}\right) \tag{3.3b}$$

According to this equation, at supersonic (M>1) the first parenthesis of the dissipation term, the third term of Eq. (3.3a), reduces to unity. In other words, the numerical dissipation introduced from this term is constant regardless of Mach number at a supersonic speed. In the previous sections, we discovered from numerical survey that the dissipation was insufficient in the original form, and this shortage will become greater for a larger Mach number (a stronger shock).

Thus, we propose here to modify this term so that the dissipation is proportional to the Mach number as follows:

$$\tilde{p} = \frac{p_L + p_R}{2} + \frac{f_p^+ - f_p^-}{2}(p_L - p_R) + \frac{1}{c_{1/2}}\sqrt{\frac{u_L^{\,2} + v_L^{\,2} + w_L^{\,2} + u_R^{\,2} + v_R^{\,2} + w_R^{\,2}}{2}}\left(f_p^+ + f_p^- - 1\right)\frac{p_L + p_R}{2} \tag{3.4}$$

Considering possible extension to real fluids [30], the above expression is improved further:

$$\tilde{p} = \frac{p_L + p_R}{2} + \frac{f_p^+ - f_p^-}{2}(p_L - p_R) + \sqrt{\frac{u_L^{\,2} + v_L^{\,2} + w_L^{\,2} + u_R^{\,2} + v_R^{\,2} + w_R^{\,2}}{2}}\left(f_p^+ + f_p^- - 1\right)\bar{\rho}c_{1/2} \tag{3.5}$$

With this new pressure flux, a new flux function named “SLAU2” has been derived.

3.4 Steady normal shock test for SLAU2

The first test here is, again, 1D and 1.5D steady normal shock problems. The results are summarized in Table 3, in which SLAU2 demonstrates an excellent performance against the shock anomalies (our experience tells that the version of $c_{1/2}$=min($c_L^{\sim}$,$c_R^{\sim}$), Eq. (2.5g), is slightly more robust than that of the arithmetic average, Eq. (2.3h), but for simplicity, for the rest of the paper, we use Eq. (2.3h) as a default $c_{1/2}$). These results are interpreted as follows: By adding more numerical dissipation to the flux for M>1, the improved scheme indeed showed robustness against the shock. Then, careful readers may speculate that more dissipative schemes simply tend to get high scores in this test, however, we stress here that the things are not that simple: Generally, too much dissipation addition to the flux yields 1D stability but in expense of Multi-D stability, as reported in [4] for Roe flux with entropy-fix [36] (included

in Table 2) or EC (Entropy Consistent)-Roe flux [37]. In addition, although more dissipative schemes such as HLLE (Harten–Lax–van_Leer–Einfeldt) [38], Van Leer's [15] or Hänel's [39] FVS, also had marked full scores in the same test sets (20 points for both 1D and 1.5D) [14], they are known to be incapable of capturing a contact discontinuity and a boundary-layer economically. Therefore, it has been extremely hard to establish a scheme which is "properly dissipative" for both shock and contact discontinuities. The present scheme "SLAU2" is such a rare example, and Fig. 8 demonstrates its boundary-layer resolution capability, in which SLAU2 reproduced Mach 0.2 Blasius' analytical velocity profile as well as SLAU and Roe, whereas HLLE, one of notoriously dissipative solvers, did not.

Flux functions and $c_{1/2}$ definitions	Test Problem	ε=0.0	0.1	0.2	0.3	0.4	0.5	0.6	0.7	0.8	0.9	Total	
SLAU2 **(default)** $[c_{1/2}=0.5(c_L+c_R)]$	1D	**2**	**2**	**2**	**2**	**2**	**2**	**2**	**2**	**2**	**2**	**20**	**40**
	1.5D	**2**	**2**	**2**	**2**	**2**	**2**	**2**	**2**	**2**	**2**	**20**	

Table 3 1D and 1.5D tests for SLAU2 flux (ε: shock location parameter [4])

4. AUSM$^+$-up2 and LDFSS2001-2: Application of new pressure flux

Now that we have derived a new pressure flux which feeds proper dissipation into a captured shock, we further consider to apply this pressure flux to other well-known AUSM-family all-speed fluxes, i.e., AUSM$^+$-up and LDFSS2001.

4.1 AUSM$^+$-up2

The dissipation in the pressure flux of AUSM$^+$-up is fed differently from SLAU or LDFSS2001: it is given by the additional term p_u of Eq. (2.4c). Since this term goes to zero for M>1 (except for a strong compression or expansion), p_u is interpreted as a dissipation term working only for low speeds. Thus, we considered to devise another way for AUSM$^+$-up to have dissipation proportional to Mach number at supersonic speeds following SLAU2. This will lead to the major modifications on the pressure flux, and there could be many options: in this study, we adopted the exactly the same pressure flux as SLAU2, namely, Eq. (3.5), and the modified flux will be referred to as "AUSM$^+$-up2."

4.2 LDFSS2001-2

The difference of the pressure flux Eq. (2.5a) in LDFSS2001 from Eq. (3.5) in SLAU2 lies only in the third term. This term controls the dissipation, but from the definition of V_{ref} in Eq. (2.5d), the dissipation amount stays constant for M>1 as in SLAU. Then, we consider replacing this term by the corresponding term of SLAU2 which is proportional to Mach number, again. This modification is equivalent to the whole replacement of Eq. (2.5a) by Eq. (3.5). We will call this modified form "LDFSS2001-2."

By using Eq. (3.5) as a) pressure flux in SLAU, AUSM$^+$-up, or LDFSS2001, instead of the original formulation, SLAU2, AUSM$^+$-up2, or LDFSS2001-2 has been established, respectively (see Fig. 4). These new schemes, summarized in Appendix for their full formulations, will be applied to numerical examples and their performances be demonstrated in the subsequent sections.

5. The two issues in hypersonic heating computations

In this section, the two issues mentioned in Introduction, "A) robustness against shock anomalies" and "B) smooth heating prediction," are investigated for the presented schemes using the new pressure flux: SLAU2, AUSM$^+$-up2, and LDFSS2001-2. As for A), hypersonic inviscid problems are employed, whereas wall heating profiles are compared for B) in a viscous blunt-body flow.

5.1 Robustness against shocks

5.1.1 1.5D steady shock problem (Euler Eqs., First-order in space)

We conducted additional cases for the 1.5D normal shock test using the newly developed flux functions as well as the original ones. The results are summarized in Table 4. From these results, one can see the new schemes SLAU2, AUSM$^+$-up2, and LDFSS2001-2 are more robust than their original counterparts, and as robust as Van

Leer's FVS. In addition, since the choice of δ=4 appears to have better performance than δ=1 for both LDFSS2001 and LDFSS2001-2, we will set δ=4 as a default value for these schemes.

Table 4. 1.5D test results for various numerical flux functions (ε: shock location parameter [4]).

Numerical Flux Functions		ε=0.0	0.1	0.2	0.3	0.4	0.5	0.6	0.7	0.8	0.9	Total
SLAU2		**2**	**2**	**2**	**2**	**2**	**2**	**2**	**2**	**2**	**2**	**20**
AUSM$^+$-up2		**2**	**2**	**2**	**2**	**2**	**2**	**2**	**2**	**2**	**2**	**20**
LDFSS2001-2	δ=1	**2**	**2**	**2**	**2**	**2**	**2**	**2**	1	**2**	**2**	19
	δ=4	**2**	**2**	**2**	**2**	**2**	**2**	**2**	**2**	**2**	**2**	**20**
SLAU		1	**2**	**2**	**2**	1	1	1	1	1	1	13
AUSM$^+$-up		**2**	**2**	**2**	**2**	**2**	1	1	1	1	**2**	16
LDFSS2001	δ=1	**2**	**2**	**2**	**2**	**2**	**2**	1	1	1	**2**	17
	δ=4	**2**	**2**	**2**	**2**	**2**	**2**	1	1	**2**	**2**	18

5.1.2 2D blunt-body problem (Euler Eqs., First-order in space)

We computed a two-dimensional blunt-body flow to confirm the robustness of each scheme shown in the 1.5D problem. The flow conditions are selected to correspond to Nagoya University Shock Tunnel, as shown in Table 5, where the radius of the cylinder (the test model) r =20mm. The computational grid has 160 (circumferential) × 80 (wall-normal) cells that are equally spaced in each direction. The grid and the coordinates are shown in Figs. 9a and 9b.

The computations were carried out with first-order both in space and time, and CFL=0.5 with an explicit time evolution. Convergence was achieved between 30,000 and 40,000 steps in each case. These solutions are visualized in Figs. 9c-9i.

The new schemes SLAU2, AUSM$^+$-up2, and LDFSS2001-2, as well as SLAU, captured the shock very smoothly (Figs. 9c-9f). On the other hand, AUSM$^+$-up showed slight oscillations in the shock shape affected by the grid line positioning relative to the shock [14] (Fig. 9g); LDFSS2001 yielded asymmetry (Fig. 9h). Thus, it is said these schemes have been improved by the present pressure flux [Eq. (3.5)] to have smoother resolution of shocks. In addition, the Roe (E-fix) flux (Roe flux [28] with Harten's entropy-fix [36]) caused the carbuncle and reached an obviously anomalous solution.

5.2 Smooth heating prediction

5.2.1 2-D blunt-body, hypersonic heating problem (Navier-Stokes Eqs., Second-order in space)

We then considered hypersonic heating on the wall of blunt-body used above. The freestream conditions (Table 5) and the model radius (r =20mm) are the same as in the previous test, though in this test the wall temperature is prescribed as T_w =300 K (isothermal wall condition), and the grid lines are clustered to the wall so that the cell Reynolds number (Reynolds number based on the minimum spacing $\Delta_{\min}$) Re_{cell} =1.3. The grid has 160 × 160 cells and shown in Figs. 10a. The coordinates are the same as in Fig. 9b.

Numerical flux functions of SLAU2, AUSM$^+$-up2, and LDFSS2001-2 are selected. Spatially second-order is guaranteed by MUSCL [34] reconstruction with Van Albada limiter [35] for the inviscid term, while central difference is used for the viscous term. For time integration, LU-SGS[5] (Lower–Upper Symmetric Gauss–Seidel) is used with CFL=200, and the computations were conducted for 100,000 steps to achieve approximately three orders reduction of the density residual.

Table 5. 2D blunt-body flow conditions.

M_∞	8.1
Re_r	1.31×10^5
P_∞ [Pa]	370.6
T_∞ [K]	63.73

The computed flowfields are displayed in Figs. 10b-10d. All the three schemes showed similar results with slight differences near the shock, and no clear evidence of carbuncles.

Figure 11 shows the corresponding wall heating profiles. The abscissa is the angle ϕ already defined in Fig. 9b, and ϕ=0 stands for

[5] The spectral radius $\sigma = |V_n| + c +$ (viscous term) is usually used, whereas some may speculate on whether it should be modified to $\sigma = |V_n| + \max(c, |V_n|) +$ (viscous term) for mathematical consistence with the new pressure flux. We confirmed that this modification has practically no effects on the solution or convergence, and hence, we adopted the conventional spectral radius $\sigma = |V_n| + c +$ (viscous term) here.

the stagnation point; the ordinate is the heat flux standardized by Fay-Riddell's stagnation value [40] of q_{FR}=17.5 W/cm^2. From this graph, as mentioned in the Introduction, SLAU2 showed a wavy pattern of heating, in spite of "A) robust capturing of the shock," "B-1) total enthalpy preserving," and "B-2) boundary-layer resolving" properties. On the contrary, AUSM$^+$-up2 and LDFSS2001-2, developed as a combination of "a) pressure flux of SLAU2 having property A," and "b) mass flux of AUSM$^+$-up or LDFSS2001 with B-1, B-2, and B-3) smooth heating profiles," produced good predictions on hypersonic heating not confined in the vicinity of the stagnation but all over the wall.

Therefore, it has been demonstrated numerically that *the new fluxes AUSM$^+$-up2 and LDFSS2001-2 using the new pressure flux in SLAU2 improved response to the shock of their original schemes* and that *they satisfy all the properties A), B-1), B-2), and B-3) for accurate heating predictions*.

6. Numerical examples

The proposed schemes using the new pressure flux, SLAU2, AUSM$^+$-up2, and LDFSS2001-2, are applied further to the following examples: a low speed flow, a three-dimensional hypersonic heating problem, and an aerodynamic analysis on a rocket having a complex geometry at a supersonic speed.

6.1 Low dissipation at low speeds

6.1.1 Low speed flow over 2-D airfoil (Euler Eqs., Second-order in space)

The present schemes are supposed to be in the family of "all-speed schemes" that have properly scaled C) low dissipation at low speeds, as well as their original fluxes SLAU, AUSM$^+$-up, and LDFSS2001. In order to confirm this property, we deal with M_∞=0.01, inviscid flow around NACA0012 airfoil with no angle of attack. Theoretically, the drag in this flow should be zero; thus, the computed drag is a good measure of numerical error [26].

Table 6. Computed drag coefficients C_d for NACA0012 airfoil.

Numerical Flux	Time Integration Method	C_d
SLAU2	pLU-SGS	0.0032
AUSM$^+$-up2	pLU-SGS	0.0037
LDFSS2001-2	pLU-SGS	0.0048
SLAU	pLU-SGS	0.0037 [26]
Roe	LU-SGS	0.0720 [26]

The grid is O-type and consists of 200 (circumferential) × 30 (wall normal) cells. The following numerical fluxes are used: SLAU2, AUSM$^+$-up2, LDFSS2001-2, SLAU (for comparison [26]), and Roe (for comparison [26]). As for time integration, LU-SGS or preconditioned LU-SGS (abbreviated as "pLU-SGS") [33] is adopted. The density residual dropped about five orders in 2,000 steps with CFL=20.

The flowfields at 2,000 steps are shown in Fig. 12, and the corresponding drag coefficients C_d in Table 6. Roe resulted in unphysical pressure contours (Fig. 12b) and huge numerical error (C_d); the new three schemes (SLAU2, AUSM$^+$-up2, and LDFSS2001-2) however, showed correct solutions (Fig. 12a, represented by SLAU2) and errors smaller than 5% of that in Roe, as in the SLAU solution. Therefore, the new schemes, while showing some variation in C_d due to different amount of dissipation fed by each scheme, attain as low dissipation as their original versions at low speeds and are applicable to such a flow regime.

6.2 3-D applications

6.2.1 3-D blunt-body, hypersonic heating problem (Navier-Stokes Eqs., Second-order in space)

This sub-subsection deals with a viscous, hypersonic (M_∞=17) benchmark test used for LAURA (Langley Aerothermodynamic Upwind Relaxation Algorithm) and FUN3D (Fully Unstructured Navier-Stokes) codes, employing a shock-aligned grid [23, 41]. The grid was provided by Dr. Peter Gnoffo, NASA Langley.[6] In this test, hypersonic heating over the three-dimensional circular-cylinder surface is computed and compared with reference data [41]. The computational conditions are as follows: V_∞ = 5000 m/s (M_∞=17), Re = 376,930 m^{-1}, ρ_∞= 0.001 kg/m^3, T_∞ = 200 K, T_w = 500 K. The cylinder radius is r = 1m and the minimum grid spacing Δ_{min} = 2.66e-6 m. With these setups, the cell Reynolds number is Re_{cell} = 1.00, ratio of Pitot pressure to free stream pressure P_{10}/P_2 = 387.6, and Fay-Riddell's [40] stagnation heating 46.5 W/cm^2 (slightly smaller than LAURA-predicted value [41] of 52 W/cm^2).

Flux functions of AUSM$^+$-up2, LDFSS2001-2, and Roe (E-fix) (for comparison [23]) are selected for this problem. The computations were conducted for 100,000 steps with LU-SGS (CFL = 200): AUSM$^+$-up2 showed four orders reduction of the density residual, whereas LDFSS2001-2 and Roe (E-fix) reached machine zero convergence.

[6] Private communication with Peter Gnoffo, NASA Langley Research Center, Mar. 2009.

Figures 13 and 14 show the computed results. From Fig. 13, symmetry and smooth shock profiles are observed for AUSM$^+$-up2 and LDFSS2001-2, in contrast to the Roe (E-fix) solution exhibiting spatial (three-dimensional) oscillation in the spanwise direction.

The heating profiles on *all* the wall elements are plotted in Fig. 14. Also shown in Fig. 14 are the corresponding two-dimensional computations (using one cell in the spanwise direction) and reference LAURA results [41]. Similar to the shock shapes in Fig. 13, heating profiles produced by AUSM$^+$-up2 and LDFSS2001-2 are as symmetry and smooth as the LAURA solutions, and accurate over the cylinder wall that are in excellent agreement with the Fay-Riddell value and the two-dimensional results; whereas Roe (E-fix) gave considerable spanwise variations at most 60% as reported in [23].

6.2.2 Aerodynamic analysis on rocket configuration at supersonic speed (Navier-Stokes Eqs., Second-order in space)

We applied our present schemes to a rocket configuration. The rocket has a complex geometry and thus, we generated an unstructured grid around it using our tool 'LS-GRID [42]' (Fig. 15; 64 million cells). Then, our unstructured grid CFD solver 'LS-FLOW [43]' was used for flow computations. The computational conditions are set as the same as the corresponding wind-tunnel test [44], i.e., M_∞=1.5, Re=1.2×10^7, the attack angle α=5 deg, and the roll angle ϕ = 60 deg. Details are found in Ref. [44].

The new schemes SLAU2, AUSM$^+$-up2, and LDFSS2001-2 are selected for inviscid flux computation, along with Green-Gauss second-order extension with Venkatakrishnan limiter [45]. Wang's method [46] is used to second-order reconstruction for viscous flux, and Spalart-Allmaras turbulence model [47] without tripping term [48] for calculation of turbulent viscosity μ_t. The steady flowfield is assumed (except for the base flow) and the local time stepping technique (CFL=1) is employed with LU-SGS. The computations are carried out on 64 processors of JAXA (Japan Aerospace Exploration Agency) Supercomputer System, JSS, for each case as in [44]. Then, the results are compared with the experiment.

Figure 16 shows a visualized computed flowfield (detailed discussions for the flowfields are not the scope of the present paper, thus omitted), represented by SLAU2 result which is indistinguishable from the results by other schemes. Any of the results captured shock waves, boundary-separations, and three-dimensional vortices generated by protuberant devices. Shown in Fig. 17 is a close-up view of computed flowfield around the rear portion device (x/L≈0.9) (again, represented by SLAU2) along with reference surface oil visualization [44]. This region is of the very rear portion of the rocket body and hence considered to be easily affected by numerical methods; nevertheless, all the three schemes shared the major flow profiles and they are consistent with the oilflow pattern.

Finally, the roll moment, considered very sensitive to the numerical method used, is compared and found within 2% variation among the proposed three schemes: This demonstrates these schemes' applicability to flows involving complex geometries.

7. Conclusions

A numerical survey on the choice of an interfacial speed of sound, denoted as $c_{1/2}$ here, was conducted for AUSM-family flux functions, and it was demonstrated that this choice did have impacts on robustness of fluxes against captured shock waves especially when $c_{1/2}$ is contained in dissipation term. Then, a new pressure flux was derived, which has modified dissipation term being proportional to upstream Mach number, in contrast to the conventional counterpart which feeds constant dissipation regardless of Mach number. The new pressure flux is applied to three AUSM-family, all-speed schemes (SLAU, AUSM$^+$-up, and LDFSS2001), and the improved schemes (SLAU2, AUSM$^+$-up2, and LDFSS2001-2) satisfy the following properties:

A) Robustness against shock anomalies (as robust as Van Leer's flux-vector-splitting)

B-1) Total enthalpy preserving

B-2) Boundary-layer resolving (An ability of the Euler solver to sharply resolve contact discontinuities)

B-3) Smooth representation of heating (AUSM$^+$-up2 and LDFSS2001-2 only)

AUSM$^+$-up2 and LDFSS2001-2 having all these properties have been demonstrated to yield accurate prediction of hypersonic heating with smooth profiles. SLAU2 result suggests that the property A (robustness against the shock) should be treated separately from B-3 (smooth heating profile), which we had originally considered as a simple outcome of A, and that satisfying A only is not sufficient for representing smooth wall heating profiles.

Furthermore, the new schemes are still applicable to low speed flows thanks to the property:

C) Low dissipation at low speeds

Numerical tests demonstrated that those schemes can be actually used for a broad spectrum of Mach numbers and also for a practical problem involving complex geometries. These fluxes have been created through numerical

investigations on $c_{1/2}$ inside numerical shock structure, in which no physical or mathematical explanation is justifiable.

We also point out that AUSM$^+$-up2 and LDFSS2001-2 require at least one user-specified reference parameter for low speeds. It is difficult to define such parameters for internal flows, for instance, in which no freestream exists. On the other hand, SLAU2 is free from this restriction. Thus, for practical usage, it is advised that the users adopt AUSM$^+$-up2 or LDFSS2001-2 for hypersonic flows or low speed flows when reference velocity is available, whereas SLAU2 is recommended for low speed flows without reference velocity; either of these three can be used for moderate speeds, as they are exactly the same as their original fluxes (that were already validated in numerous applications) for subsonic flows, and almost unchanged for moderate supersonic speeds.

In addition, although SLAU2, AUSM$^+$-up2 and LDFSS2001-2 are as robust as Van Leer's flux-vector-splitting against shock anomalies, it should be warned that all of them still have potentials to trigger the carbuncle under an extreme condition. This would possibly be suppressed (at least partly) by multidimensional dissipation as in Refs. [41] and [49-52]. Nevertheless, we believe the present work placed a milestone for future developments.

Therefore, as a future work, we will design a unified scheme which is more robust than AUSM$^+$-up2 and LDFSS2001-2, and needs no tunable parameters as SLAU2, possibly equipped with a multidimensional stabilization term. Then, the scheme will be extended to multiphase flows [53] and other applications.

Acknowledgments

This work was inspired and motivated by discussions with Dr. Hiroaki Nishikawa, National Institute of Aerospace, and Dr. Jeffery White, NASA Langley, and by a valuable comment by Assistant Prof. Taku Nonomura, JAXA. The 1.5D test was studied while Keiichi Kitamura, the first author, spent a year at University of Michigan, Ann Arbor, MI, under supervision of Prof. Philip L. Roe. Dr. Peter Gnoffo, NASA Langley, provided us with a computational grid used in the Mach 17, three-dimensional circular-cylinder benchmark. One of the computational codes was originally developed at Nagoya University, Japan, while Keiichi Kitamura studied at Prof. Yoshiaki Nakamura's laboratory. The unstructured grid generation tool "LS-GRID" and the solver "LS-FLOW" used for a rocket configuration were developed by Dr. Keiichiro Fujimoto and Dr. Kazuto Kuzuu with the authors at JEDI center, JAXA, Japan. Prof. Z.J. Wang at Iowa State University (currently Spahr Professor and Chair at University of Kansas) and Mr. Junya Aono at Research Center of Computational Mechanics, Inc., Japan, also helped us developing the codes. Dr. Fujimoto also gave us comments on the draft of this paper. The experiment for the rocket was conducted in collaboration with Associate Prof. Satoshi Nonaka, Ms. Tomoko Irikado, Dr. Keiichiro Fujimoto, Dr. Kazuto Kuzuu, Mr. Yuji Ohya, Associate Prof. Akira Oyama, Mr. Moriyasu Fukuzoe, Mr. Kazuyuki Miho, and Mr. Makoto Tamura at JAXA. Dr. Meng-Sing Liou, NASA Glenn, gave us valuable comments on this work. We are grateful to all their cooperation.

Appendix: Formulation of SLAU2, AUSM$^+$-up2, and LDFSS2001-2

The AUSM-family fluxes are generally written as

$$\mathbf{F}_{1/2} = \frac{\dot{m}+|\dot{m}|}{2}\boldsymbol{\Psi}^+ + \frac{\dot{m}-|\dot{m}|}{2}\boldsymbol{\Psi}^- + \tilde{p}\mathbf{N} \tag{A.1a}$$

$$\boldsymbol{\Psi} = (1, u, v, w, H)^T, \quad \mathbf{N} = (0, n_x, n_y, n_z, 0)^T \tag{A.1b}$$

Then, the new pressure flux introduced in this paper is

$$\tilde{p} = \frac{p_L + p_R}{2} + \frac{f_p^+ - f_p^-}{2}(p_L - p_R) + \sqrt{\frac{u_L^{\,2} + v_L^{\,2} + w_L^{\,2} + u_R^{\,2} + v_R^{\,2} + w_R^{\,2}}{2}}\left(f_p^+ + f_p^- - 1\right)\bar{\rho}c_{1/2} \tag{A.2}$$

and the choice of its partner mass flux determines the complete form of the flux function.

SLAU2 (and SLAU):

$$\dot{m} = \frac{1}{2}\left\{\rho_L\left(V_{nL} + |\bar{V}_n|^+\right) + \rho_R\left(V_{nR} - |\bar{V}_n|^-\right) - \frac{\chi}{c_{1/2}}\Delta p\right\} \tag{A.3a}$$

$$|\bar{V}_n|^+ = (1-g)\,|\bar{V}_n| + g\,|V_{nL}|, \quad |\bar{V}_n|^- = (1-g)\,|\bar{V}_n| + g\,|V_{nR}| \tag{A.3b}$$

$$\left|\overline{V}_n\right| = \frac{\rho_L\left|V_{nL}\right| + \rho_R\left|V_{nR}\right|}{\rho_L + \rho_R} \tag{A.3c}$$

$$g = -\max\left[\min\left(M_L, 0\right), -1\right] \cdot \min\left[\max\left(M_R, 0\right), 1\right] \quad \in [0, 1] \tag{A.3d}$$

where definition of the interfacial speed of sound $c_{1/2}$ is borrowed from AUSM$^+$.

$$c_{1/2} = \min\left(\tilde{c}_L, \tilde{c}_R\right), \quad \tilde{c}_{L/R} = c^{*2} \Big/ \max\left(c^*, \left|V_n^{\pm}\right|\right), \; c^{*2} = \frac{2(\gamma-1)}{(\gamma+1)} H \tag{A.3e}$$

No user-specified value is involved.

AUSM$^+$-up2 (and AUSM$^+$-up):

$$\dot{m} = M_{1/2} c_{1/2} \begin{cases} \rho_L & \text{if } M_{1/2} > 0 \\ \rho_R & \text{otherwise} \end{cases} \tag{A.4a}$$

$$M_{1/2} = f_M{}^{+} + f_M{}^{-} + M_p \tag{A.4b}$$

$$f_M^{\pm} = \begin{cases} \dfrac{1}{2}\left(M \pm |M|\right), & \text{if } |M| \geq 1 \\ \pm\dfrac{1}{4}\left(M \pm 1\right)^2 \pm \dfrac{1}{8}\left(M^2 - 1\right)^2, & \text{otherwise} \end{cases} \tag{A.4c}$$

$$M_p = -\frac{K_p}{f_a} \max\left(1 - \sigma \overline{M}^2, 0\right) \frac{p_R - p_L}{\bar{\rho} c_{1/2}^2}, \quad \bar{\rho} = \frac{\rho_L + \rho_R}{2} \tag{A.4d}$$

where

$$c_{1/2} = \min\left(\tilde{c}_L, \tilde{c}_R\right), \quad \tilde{c}_L = c^{*2} \Big/ \max\left(c^*, V_n{}^{+}\right), \quad \tilde{c}_R = c^{*2} \Big/ \max\left(c^*, -V_n{}^{-}\right) \tag{A.4e}$$

$$c^{*2} = \frac{2(\gamma-1)}{(\gamma+1)} H \tag{A.4f}$$

$$\alpha = \frac{3}{16}\left(-4 + 5 f_a^2\right) \tag{A.4g}$$

$$f_a\left(M_o\right) = M_o\left(2 - M_o\right) \tag{A.4h}$$

$$M_o{}^2 = \min\left(1, \max\left(\overline{M}^2, M_\infty^2\right)\right) \tag{A.4i}$$

$$\overline{M}^2 = \frac{V_n{}^{+2} + V_n{}^{-2}}{2 c_{1/2}^2} \tag{A.4j}$$

and tunable parameters are K_u=0.75, K_p=0.25, σ=1.0, and uniform Mach number, M_∞.

LDFSS2001-2 (and LDFSS2001):

$$\tilde{\mathbf{F}} = \dot{m}^{+}\boldsymbol{\Psi}^{+} + \dot{m}^{-}\boldsymbol{\Psi}^{-} + \tilde{p}\mathbf{N} \tag{A.5a}$$

$$\dot{m}^{+} = \rho_L \tilde{c}_{1/2}\left(f_M^{+} - f_{1/2}^{+}\right), \; \dot{m}^{-} = \rho_R \tilde{c}_{1/2}\left(f_M^{-} + f_{1/2}^{-}\right) \tag{A.5b}$$

$$f_M^{\pm} = \begin{cases} \dfrac{1}{2}\left(M \pm |M|\right), & \text{if } |M| \geq 1 \\ \pm\dfrac{1}{4}\left(M \pm 1\right)^2, & \text{otherwise} \end{cases} \tag{A.5c}$$

$$f_{1/2}^{+} = f_{1/2}\left(1 - \frac{\left[\Delta p + \delta|\Delta p|\right]}{2\rho_L V_{ref,1/2}^2}\right), \quad f_{1/2}^{-} = f_{1/2}\left(1 + \frac{\left[\Delta p - \delta|\Delta p|\right]}{2\rho_R V_{ref,1/2}^2}\right), \ \delta \in [0,4], \ \ \Delta p = p_L - p_R$$

$$f_{1/2} = \begin{cases} \frac{1}{4}\left[\sqrt{\frac{1}{2}\left(M_L^2 + M_R^2\right)} - 1\right]^2, & if \ |M_L| < 1, |M_R| < 1 \\ 0, & otherwise \end{cases} \tag{A.5d}$$

where δ=4 in this study,

$$M_{L/R} = V_n^{\pm} / \tilde{c}_{1/2}, \quad \tilde{c}_{1/2} = \sqrt{\tilde{c}_L \cdot \tilde{c}_R}, \quad \tilde{c}_{L/R} = \frac{\sqrt{V_n^{\pm 2}\left(1 - M_{ref}^2\right)^2 + 4V_{ref}^2}}{1 + M_{ref}^2} \tag{A.5e}$$

$$M_{ref}^2 = V_{ref}^2 / {c_{1/2}}^2, \quad V_{ref}^2 = \min\left({c_{1/2}}^2, \max\left(|\vec{V}|^2, V_\infty^2\right)\right), \ |\vec{V}|^2 = u^2 + v^2 + w^2 \tag{A.5f}$$

$$c_{1/2} = \min\left(c_L, c_R\right), \quad c_{L/R} = c^{*2} / \max\left(c^*, |V_n^{\pm}|\right), \ c^{*2} = \frac{2(\gamma - 1)}{(\gamma + 1)} H \tag{A.5g}$$

and V_∞ is uniform velocity specified by a user.

References

[1] Peery, K.M. and Imlay, S.T., "Blunt-Body Flow Simulations," AIAA Paper 88-2904, 1988.

[2] Pandolfi, M. and D'Ambrosio, D.: Numerical Instabilities in Upwind Methods: Analysis and Cures for the "Carbuncle" Phenomenon, *Journal of Computational Physics*, Vol. 166, No. 2, 2001, pp.271-301.

[3] Quirk, J.J.: A Contribution to the Great Riemann Solver Debate, *Int. J. Numer. Methods in Fluids*, 18, pp.555-574 (1994).

[4] Kitamura, K., Roe, P., and Ismail, F.: Evaluation of Euler Fluxes for Hypersonic Flow Computations, *AIAA Journal*, Vol. 47, No.1, 2009, pp.44-53.

[5] Gnoffo, P., Buck, G., Moss, J., Nielsen, E., Berger, K., and Jones, W.T., "Aerothermodynamic Analyses of Towed Ballutes," AIAA Paper 2006-3771, 2006.

[6] Xu, K. and Li, Z.: Dissipative Mechanism in Godunov-type Schemes, *Int. J. Numer. Methods in Fluids*, 37, pp.1-22 (2001).

[7] Liou, M.S.: Mass Flux Schemes and Connection to Shock Instability, *J. Comput. Phys.*, 160, pp.623–648 (2000).

[8] Robinet, J.-Ch., Gressier, J., Casalis, G., and Moschetta, J.-M.: Shock Wave Instability and the Carbuncle Phenomenon: Same Intrinsic Origin?, *J. Fluid Mech.*, 417, pp. 237-263 (2000).

[9] Coulombel, J.F., Benzoni-Gavage, S., and Serre, D.: Note on a Paper by Robinet, Gressier, Casalis & Moschetta, *J. Fluid Mech.*, 469, pp. 401-405 (2002).

[10] Elling, V.: The Carbuncle Phenomenon is Incurable, *Acta Mathematica Scientia*, 29B, pp.1647-1656 (2009).

[11] Ramalho, M.V.C. and Azevedo, J.L.F., "A Possible Mechanism for the Appearance of the Carbuncle Phenomenon in Aerodynamic Simulations," AIAA Paper 2010-872, 2010.

[12] Liou, M.S., "Open Problems in Numerical Fluxes: Proposed Resolutions," AIAA Paper 2011-3055, 2011.

[13] Liou, M.S.: A Sequel to AUSM, Part II: AUSM$^+$-up for all speeds, *J. Comput. Phys.*, 214, pp.137-170 (2006).

[14] Kitamura, K., Shima, E., Nakamura, Y., and Roe, P.: Evaluation of Euler Fluxes for Hypersonic Heating Computations, *AIAA Journal*, Vol.48, No.4, 2010, pp.763-776.

[15] Van Leer, B.: Flux-Vector Splitting for the Euler Equations, *Lecture Notes in Physics*, 170, pp.507–512 (1982).

[16] Roe, P., "Vorticity Capturing," AIAA Paper 2001-2523, 2001.

[17] Chauvat, Y., Moschetta, J.M., and Gressier, J.: Shock Wave Numerical Structure and the Carbuncle Phenomenon, *Int. J. Numer. Methods in Fluids*, 47, pp.903–909 (2005).

[18] Barth, T.J., "Some Notes on Shock-Resolving Flux Functions Part 1: Stationary Characteristics," NASA TM-101087 (1989).

[19] Roe, P.L.: Fluctuations and Signals—A Framework for Numerical Evolution Problems, Numerical Methods for Fluid Dynamics, edited by K. W. Morton, and M. J. Baines, Academic Press, New York, 1982, pp. 219–257.

[20] Sanders, R., Morano, E., and Druguetz, M.C.: Multidimensional Dissipation for Upwind Schemes: Stability and Applications to Gas Dynamics, *J. Comput. Phys.*, 145, pp.511-537 (1998).

[21] Paciorri, R. and Bonfiglioli, A.: A Shock-Fitting Technique for 2D Unstructured Grids, *Computers & Fluids*, 38, pp.715-726 (2009).

[22] Paciorri, R. and Bonfiglioli, A.: Shock interaction computations on unstructured, two-dimensional grids using a shock-fitting technique, *J. Comput. Phys.*, 230, pp.3155–3177 (2011).

[23] Kitamura, K., Shima, E., and Roe, P., "Carbuncle Phenomena and Other Shock Anomalies in Three Dimensions," *AIAA J.*, Vol. 50, No. 12, 2012, pp.2655-2669. doi:10.2514/1.J051227

[24] Liou, M.S.: A Sequel to AUSM: AUSM$^+$, *J. Comput. Phys.*, 129, pp.364–382 (1996).

[25] Shima, E. and Kitamura, K., "Parameter-Free Simple Low-Dissipation AUSM-Family Scheme for All Speeds," *AIAA J.*, Vol. 49 (2011), pp.1693-1709. doi:10.2514/1.55308

[26] Kitamura, K., Shima, E., Fujimoto, K., and Wang, Z.J.: Performance of Low-Dissipation Euler Fluxes and Preconditioned LU-SGS at Low Speeds, *Communications in Computational Physics*, Vol.10 (2011), pp.90-119. doi:10.4208/cicp.270910.131110a.

[27] Liou, M.S. and Edwards, J.R., "Numerical Speed of Sound and Its Application to Schemes for All Speeds," NASA-TM-209286, 1989; AIAA Paper 99-3268-CP, 1989.

[28] Roe, P.L.: Approximate Riemann Solvers, Parameter Vectors, and Difference Schemes, *J. Comput. Phys.*, 43, pp.357–372 (1981).

[29] Henderson, S.J.. and Menart, J.A., "Grid Study on Blunt Bodies with the Carbuncle Phenomenon," AIAA Paper 2007-3904, 2007.

[30] Mazaheri, A.R. and Kleb, B., "Exploring Hypersonic, Unstructured-Grid Issues through Structured Grids," AIAA Paper 2007-4462, 2007.

[31] Edwards, J.R., "Towards Unified CFD Simulation of Real Fluid Flows," AIAA Paper 2001-2524, 2001.

[32] Li, J., Li, Q., and Xu, K.: Comparison of the generalized Riemann solver and the gas-kinetic scheme for inviscid compressible flow simulations, *Journal of Computational Physics*, Vol. 230, 2011, pp.5080-5099.

[33] Weiss, J.M. and Smith, W.A.: Preconditioning Applied to Variable and Constant Density Flows, *AIAA Journal*, Vol. 33, No.11, 1995, pp. 2050-2057.

[34] Van Leer, B.: Towards the Ultimate Conservative Difference Scheme. V. A Second-Order Sequel to Godunov's Method, *Journal of Computational Physics*, Vol. 32, 1979, pp.101-136.

[35] Van Albada, G.D., Van Leer, B. and Roberts, Jr., W.W.: A Comparative Study of Computational Methods in Cosmic Gas Dynamics, *Astron. Astrophys.*, Vol. 108, 1982, pp.76-84.

[36] Harten, A.: High Resolution Schemes for Hyperbolic Conservation Laws, *Journal of Computational Physics*, Vol. 49, 1983, pp.357-393.

[37] Ismail, F. and Roe, P.L.: Affordable, Entropy-Consistent Euler Flux Functions II: Entropy Production at Shocks, *J. Comput. Phys.*, 228, pp.5410-5436 (2009).

[38] Einfeldt, B.: On Godunov-Type Methods for Gas Dynamics, *SIAM Journal on Numerical Analysis*, 25, pp.294-318 (1998).

[39] Hänel, D. Schwane, R. and Seider, G., "On the Accuracy of Upwind Schemes for the Solution of the Navier-Stokes Equations," AIAA Paper 87-1105, 1987.

[40] Fay, J.A. and Riddell, F.R.: Theory of Stagnation Point Heat Transfer in Dissociated Air, *Journal of Aeronautical Sciences*, Vol. 25, 1958, pp.73-85.

[41] Gnoffo, P.A., "Multidimensional, Inviscid Flux Reconstruction for Simulation of Hypersonic Heating on Tetrahedral Grids," AIAA Paper 2009-599, 2009.

[42] Fujimoto, K., Fujii, K., Wang, Z.J., Kitamura, K., "Advanced Cartesian Grid-based CFD Approach for High Reynolds number Turbulent Flows," IMECE2008-67110, ASME International Mechanical Engineering Congress & Exposition, Boston, MA, 2008.

[43] Kitamura, K., Fujimoto, K., Shima, E., Kuzuu, K., and Wang, Z.J.: Validation of an Arbitrary Unstructured CFD Code for Aerodynamic Analyses, *Trans. Jpn. Soc. Aeronaut. Space Sci.*, Vol. 53 (2011), pp.311-319.

[44] Kitamura, K., Nonaka, S., Kuzuu, K., Aono, J., Fujimoto, K., and Shima, E.: Numerical and Experimental Investigations of Epsilon Launch Vehicle Aerodynamics at Mach 1.5, *J. Spacecraft and Rockets*, (Accepted).

[45] Venkatakrishnan, V.: Convergence to Steady State Solutions of the Euler Equations on Unstructured Grids with Limiters, *Journal of Computational Physics*, Vol. 118, 1995, pp.120-130.

[46] Wang, Z.J.: A Quadtree-based Adaptive Cartesian/Quad Grid Flow Solver for Navier-Stokes Equations, *Computers and Fluids*, Vol. 27, 1998, pp. 529-549.

[47] Spalart, P.R. and Allmaras, S.R., "A One-Equation Turbulence Model for Aerodynamic Flows," AIAA Paper 92-0439, 1992.

[48] Rumsey, C.L.: Apparent Transition Behavior of Widely-used Turbulence Models, *Int. J. Heat and Fluid Flow*, 28 (2007), pp. 1460-1471. doi:10.1016/j.ijheatfluidflow.2007.04.003

[49] Nishikawa, H. and Kitamura, K.: Very Simple, Carbuncle-Free, Boundary-Layer Resolving, Rotated-Hybrid Riemann Solvers, *Journal of Computational Physics*, Vol. 227, 2008, pp. 2560-2581.

[50] Shima, E. and Kitamura, K., "Multidimensional Numerical Noise from Captured Shockwave and Its Cure," *AIAA J.*, (Accepted)

[51] Loh, C.Y. and Jorgenson, P.C.E.: Multi-dimensional Dissipation for Cure of Pathological Behaviors of Upwind Scheme, *Journal of Computational Physics*, Vol. 228, 2009, pp.1343-1346.

[52] Yoon, S.H., Kim, C., and Kim, K.H.: Multi-Dimensional Limiting Process for Three-Dimensional Flow Physics Analyses, *Journal of Computational Physics*, Vol. 227, 2008, pp.6001-6043.

[53] Liou, M.S., Chang, C.H., Nguyen, L., and Theofanous, T.G.: How to Solve Compressible Multifluid Equations - A Simple, Robust, and Accurate Method, *AIAA Journal*, Vol. 46, No.9, 2008, pp. 2345-2356.

List of Figures

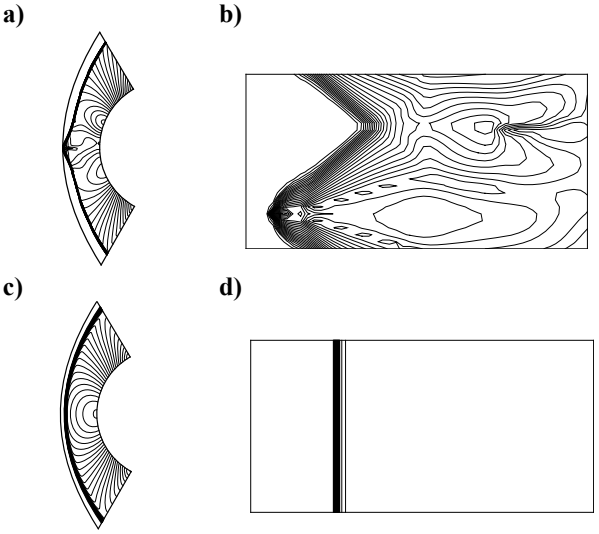

Figure 1. a), b) Carbuncle and c), d) "correct" solutions.

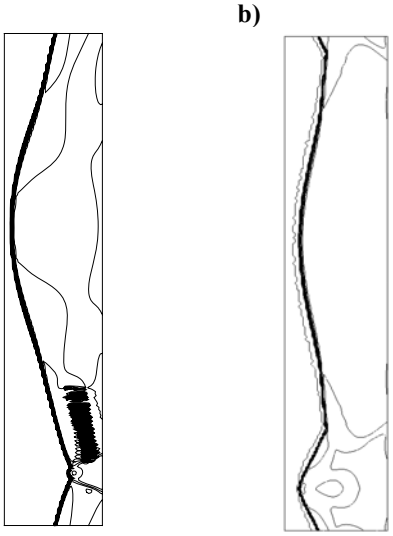

Figure 2. Carbuncles in modified 1.5D test #3 (50 × 250 cells) of [14] a) Van Leer's FVS [15], b) AUSM$^+$-up [13].

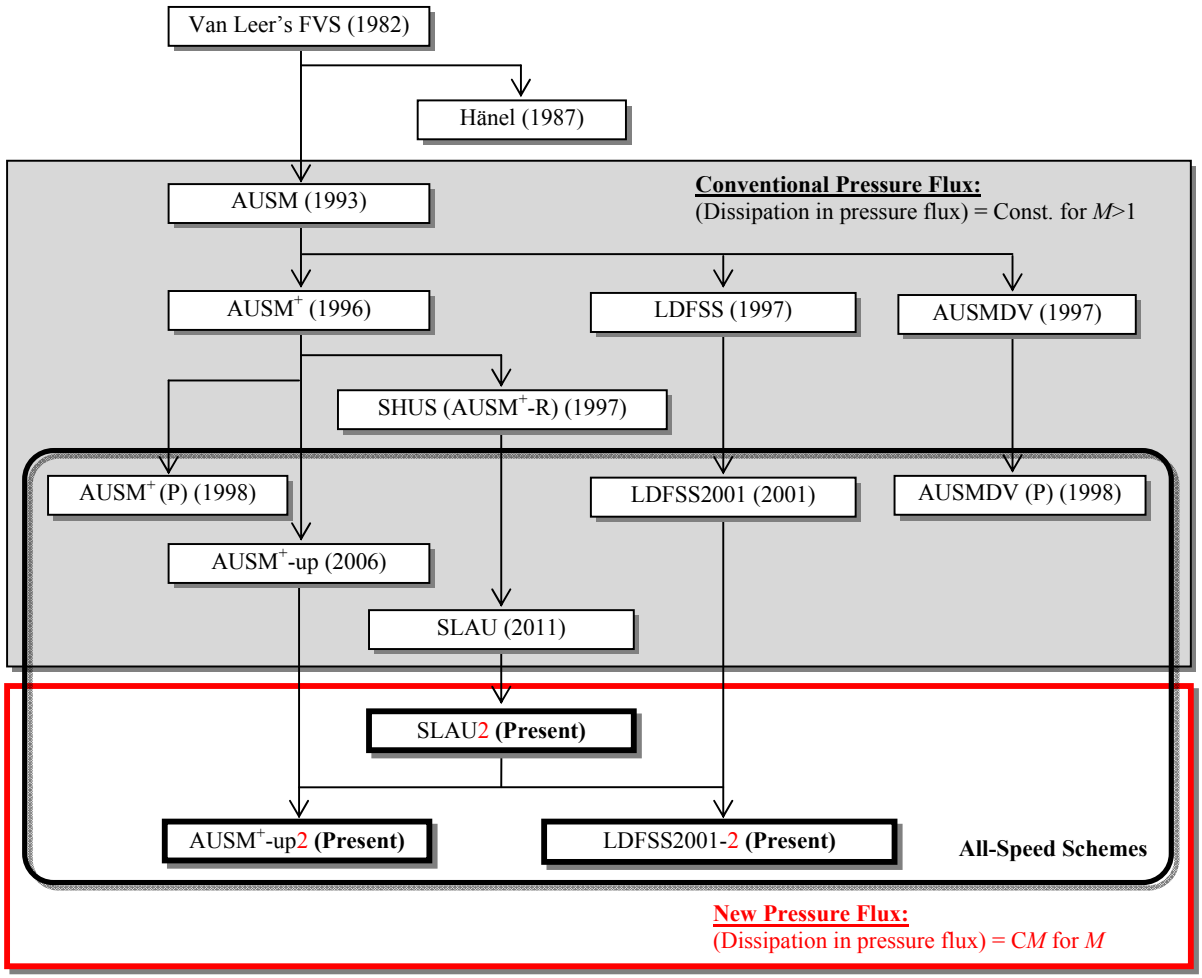

Figure 3. Evolution of Van Leer's FVS and AUSM-family schemes related to the present work.

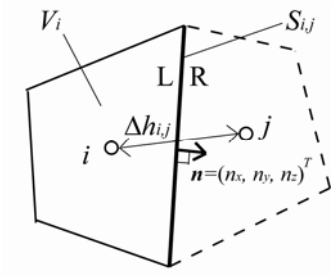

Figure 4. Schematic of cell geometric properties.

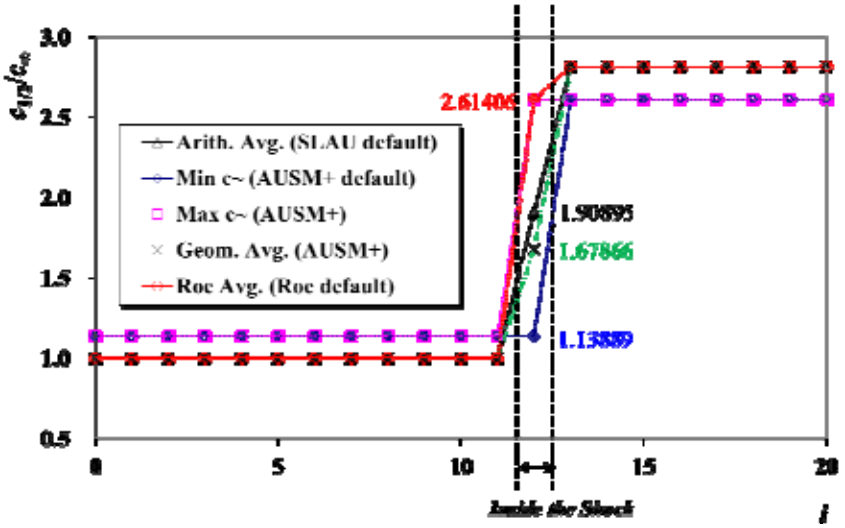

Figure 5. Interfacial speed of sound $c_{1/2}$ [standardized by freestream (= preshock) speed of sound, c_∞] with different definitions for normal shock.

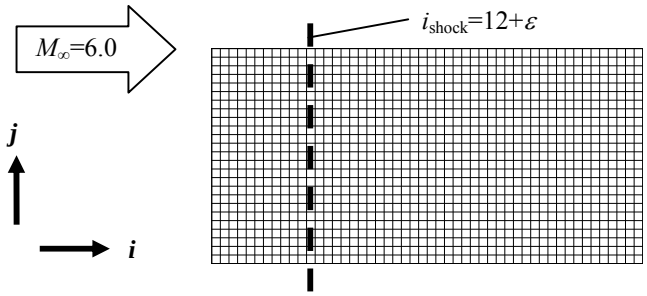

Figure 6. Computational grid and conditions for 1.5D steady normal shock test.

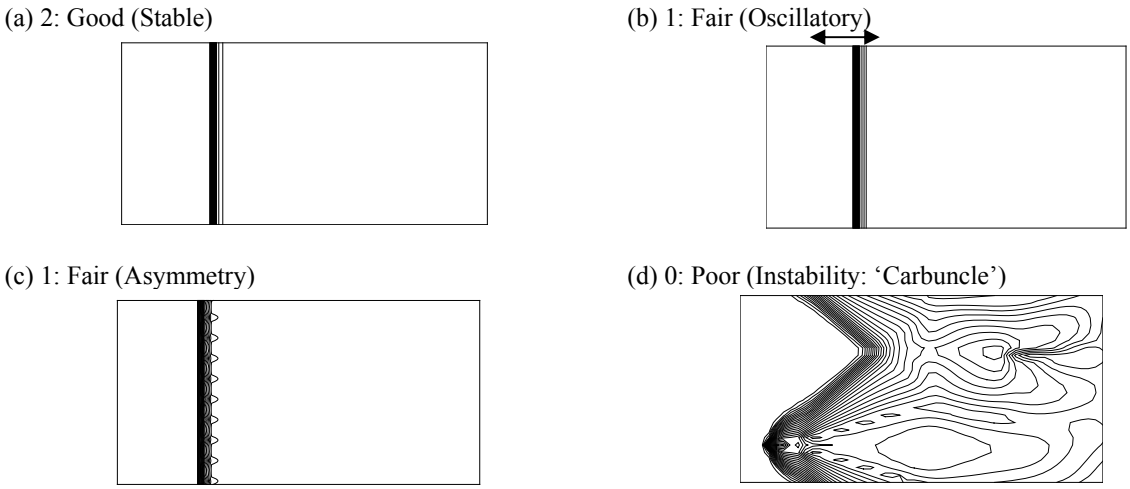

Figure 7. Typical solutions for 1.5 dimensional steady shock test.

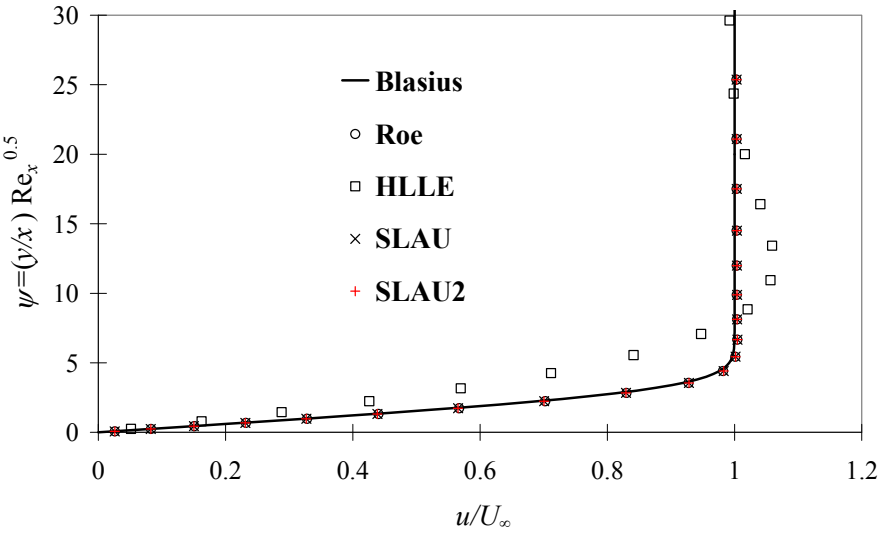

Figure 8. Velocity profiles over flat plate at $Re_x=2.2\times10^4$ for $M_\infty=0.2$, $\alpha=0$ degree (Second-order spatial accuracy, CFL=0.5).

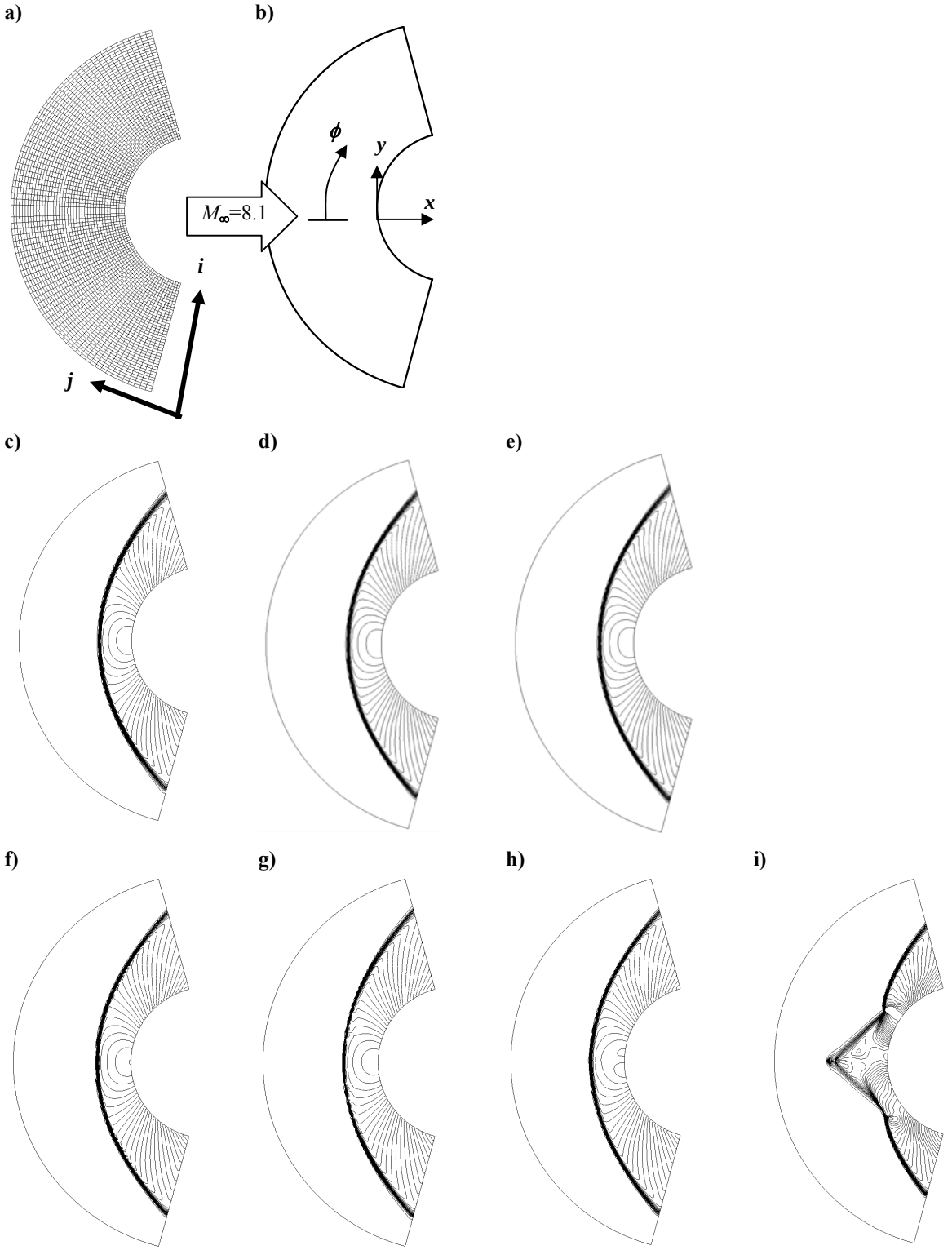

Figure 9. Hypersonic, inviscid, 2D blunt-body problem a) grid (160×80; every other grid lines are shown), b) coordinates, and results (Cp contours of converged solutions) of c) SLAU2, d) AUSM$^+$-up2, e) LDFSS2001-2, f) SLAU [25], g) AUSM$^+$-up, h) LDFSS2001, i) Roe (E-fix) [25].

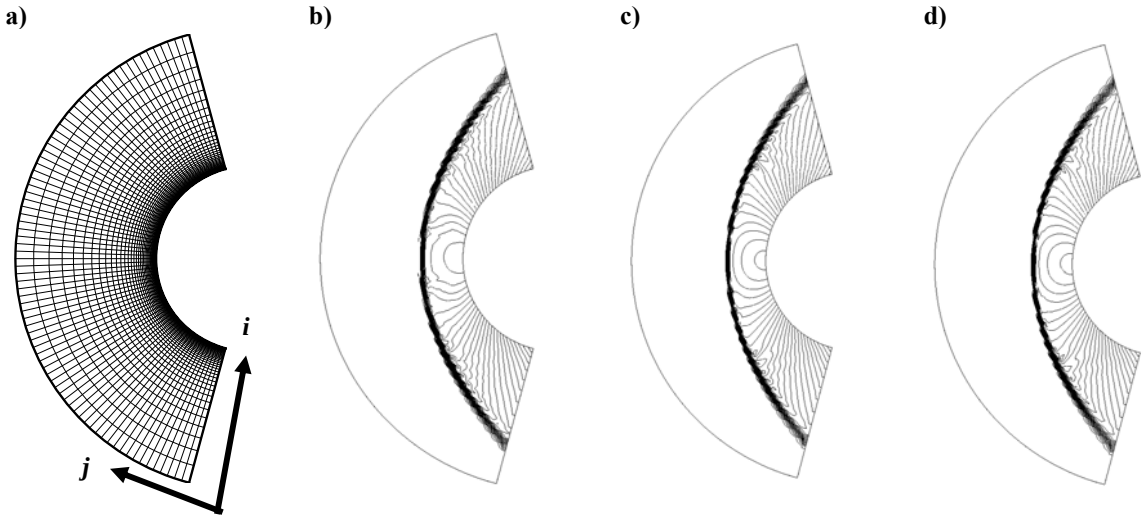

Figure 10. Hypersonic, viscous, 2D blunt-body problem a) grid (160×160; every other grid lines are shown), and results (Mach number contours at 100,000 steps) of b) SLAU2, c) AUSM$^+$-up2, d) LDFSS2001-2.

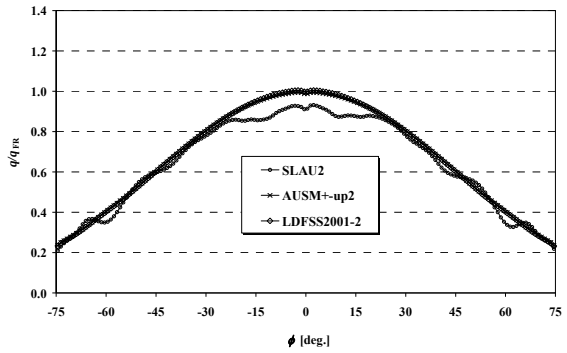

Figure 11. Aerodynamic heating profiles over a blunt-body at Mach 8.1.

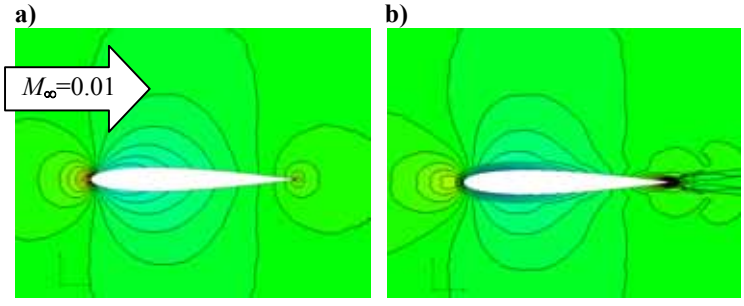

Figure 12. Cp contours (0 < Cp < 390) for low speed flow over NACA0012 airfoil (M_∞=0.01), a) SLAU2, b) Roe [26].

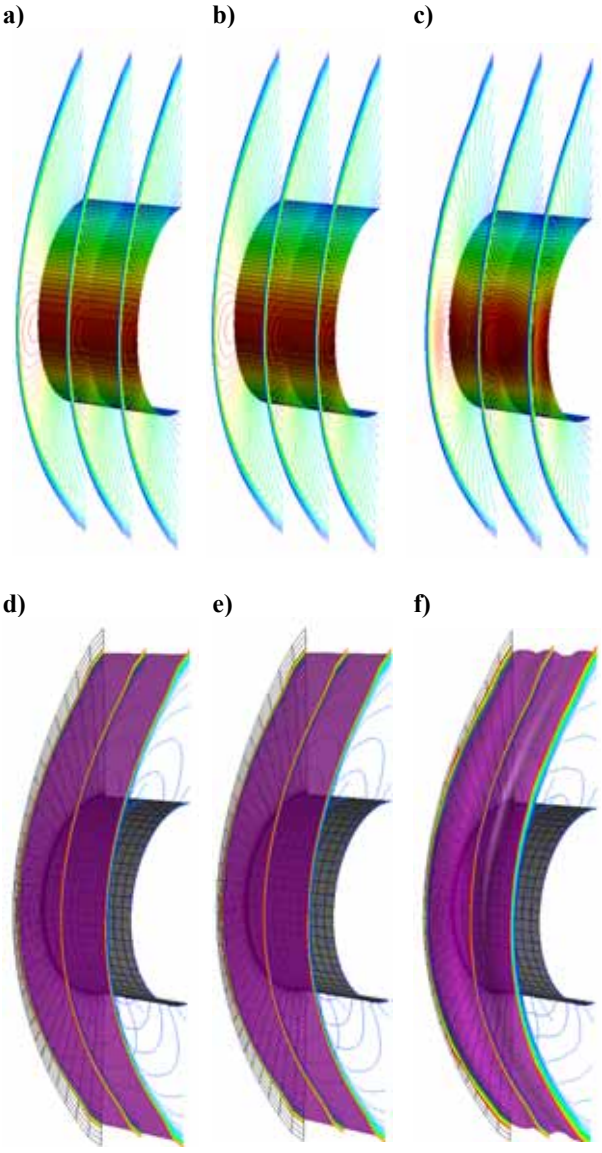

Figure 13. Pressure contours (top; $0 < P/P_\infty < 390$): a) AUSM$^+$-up2, b) LDFSS2001-2, c) Roe (E-fix) [23] and Mach number (bottom; $0 < M_\infty < 17$) contours : d) AUSM$^+$-up2, e) LDFSS2001-2, f) Roe (E-fix) [23] for 3D circular-cylinder (second-order in space; freestream Mach number M_∞=17).

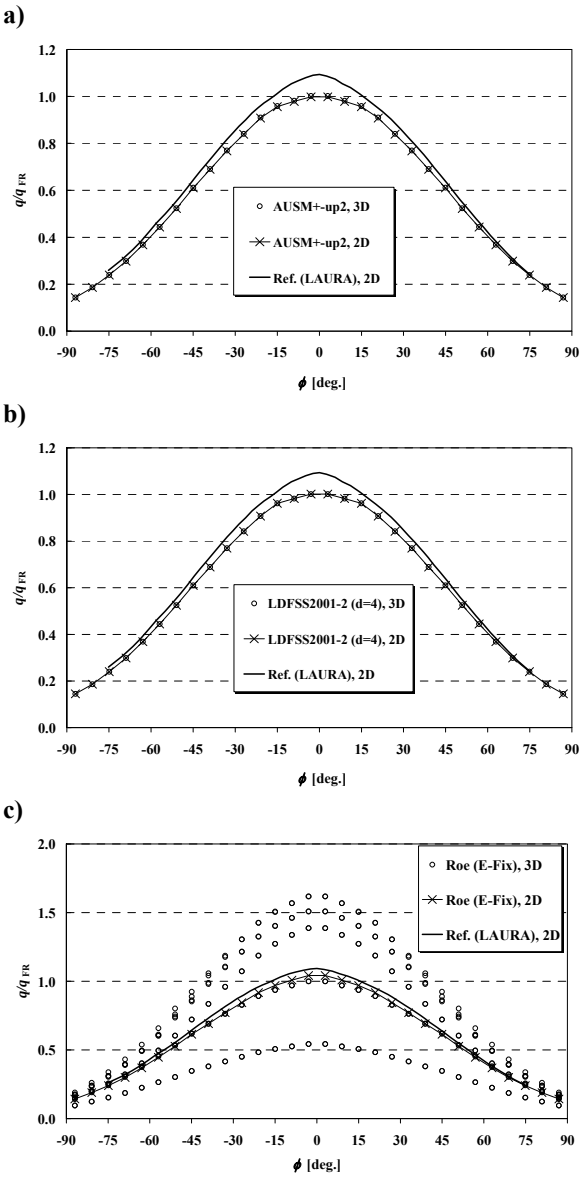

Figure 14. Aerodynamic heating profiles over blunt-body at Mach 17, a) AUSM$^+$-up2, b) LDFSS2001-2, c) Roe (E-fix) [23].

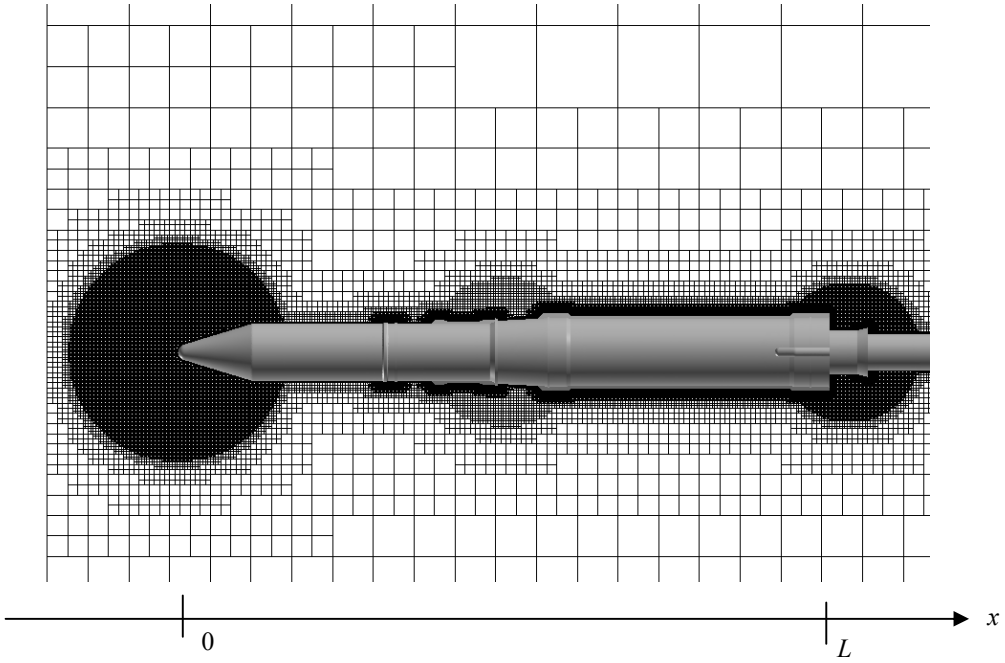

Figure 15. Computational grid (Cartesian/body-fitted hybrid, unstructured grid) generated by using LS-GRID for rocket configuration [44].

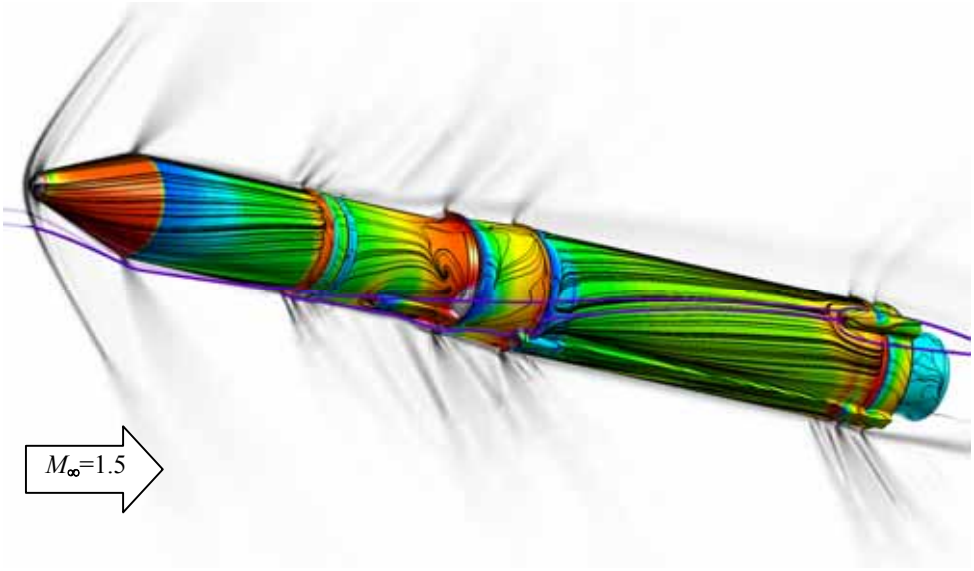

Figure 16. Computational results for rocket configuration at Mach 1.5 by SLAU2. Body: Cp contours (-0.5<Cp<0.5) with body-constraint streamlines; Flow: absolute density gradient with streamlines.

a) **b)**

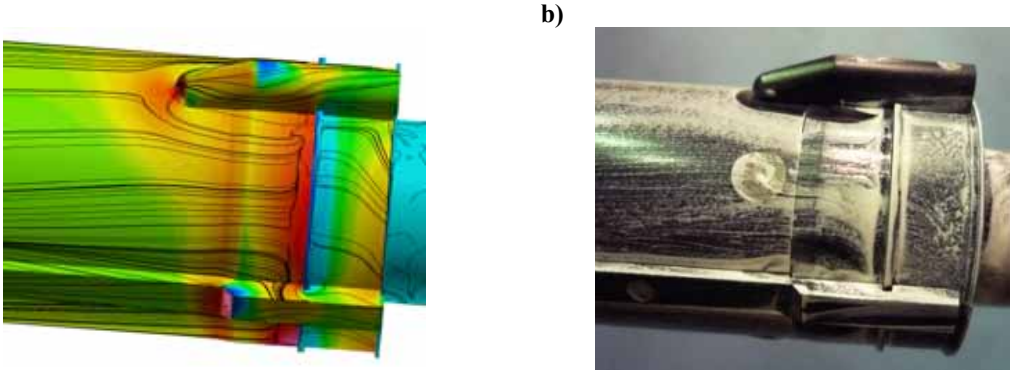

Figure 17. Computational and reference experimental results for rocket configurations at Mach 1.5 (close-up views for rear portion), a) SLAU2, b) Experimental surface oil visualization [44]. Cp contours (-0.5<Cp<0.5) with body-constraint streamlines.